

Effect of processing conditions on the properties of nanostructured BiFeO₃ obtained using different synthetic strategies

M.Usha Rani
(MS12M1005)

A Dissertation Submitted to
Indian Institute of Technology Hyderabad
In Partial Fulfillment of the Requirements for
The Degree of Master of Technology



भारतीय प्रौद्योगिकी संस्थान हैदराबाद
Indian Institute of Technology Hyderabad

Department of Materials Science & Metallurgical Engineering

December, 2014

Declaration

I declare that this written submission represents my ideas in my own words, and where others' ideas or words have been included, I have adequately cited and referenced the original sources. I also declare that I have adhered to all principles of academic honesty and integrity and have not misrepresented or fabricated or falsified any idea/data/fact/source in my submission. I understand that any violation of the above will be a cause for disciplinary action by the Institute and can also evoke penal action from the sources that have thus not been properly cited, or from whom proper permission has not been taken when needed.

M. Usha Rani

(Signature)

M.Usha Rani

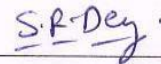
MS12M1005

Approval Sheet

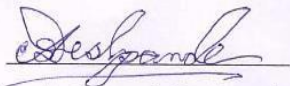
This thesis entitled "Effect of processing conditions on the properties of nanostructured BiFeO₃ obtained using different synthetic strategies" by M.Usha Rani is approved for the degree of Master of Technology from IIT Hyderabad.



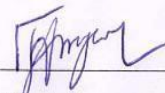
Dr. Ranjith Ramadurai
Assistant Professor
Department of Materials Science and Metallurgical Engineering
Examiner



Dr. Suhash Ranjan Dey
Assistant Professor
Department of Materials Science and Metallurgical Engineering
Examiner



Dr. Atul Suresh Deshpande
Assistant Professor
Department of Materials Science and Metallurgical Engineering
Adviser



Dr. J. Suryanarayana
Assistant Professor
Department of Physics
Chairman

Acknowledgements

Firstly my sincere thanks to my guide **Dr. Atul Suresh Deshpande**, Assistant Professor, Department of Materials Science and Metallurgical Engineering, IIT Hyderabad for his valuable guidance, strong motivation and constant encouragement during the course of this work. I also thank him for introducing me to the area of research.

I express my sincere gratitude to **Dr. Ranjith Ramadurai** for his expert guidance and support in magnetic characterization.

I would like to express my gratitude to **Dr. Mudrika Khandelwal** for guiding me in this work. I would like to acknowledge **Dr. Pinaki Prasad Battacharjee, Dr. Suhash Ranjan Dey, Dr. Bharat Bhooshan Panigrahi** and other faculty members of MSME department for supporting me throughout my thesis work.

I wish to convey my sincere thanks to **Mr. Kumaraswamy, Mr. Damodhar, Mr. Mallesh, Mr. Venkat, and Mr. Anandkumar** for helping me in characterization related works.

I would like to thank to all my M.Tech friends **Vasundhara, Nida, Bhadak balachandra, Tushar, Ankith, Rahul, Manish and Satyanarayana**.

Finally I would like to thank to my family members who had supported me in many ways in order to complete my project successfully.

Dedicated
To
My
Family

Abstract

The synthesis parameters such as pH, concentration, precipitating agents, surfactant etc., determine the single phase formation of Bismuth ferrite [BiFeO_3 (BFO)] nanoparticles via wet chemical route. By tuning the above processing conditions, different particle sizes and shape (morphology) can be synthesized which tailors the properties such as magnetic, optical etc. Single phase BFO nanoparticles were prepared through co-precipitation method using different precipitating agents such as ammonium hydroxide (NH_4OH) and tetra methyl ammonium hydroxide (TMAOH). The effect of precipitating agents on crystallite size, morphology, phase evolution and magnetic properties at constant pH were studied using XRD, FESEM, PPMS, and RAMAN. Single phase BFO was obtained in both cases by calcination at 650°C . Variation in the crystallite size using different precipitating agents (118 nm and 75 nm for NH_4OH and TMAOH respectively) was observed. Similarly, size obtained from FESEM shows $196\pm 115\text{nm}$ and $207\pm 50\text{nm}$ for NH_4OH and TMAOH respectively indicating that the actual particles are polycrystalline. Samples calcined at lower temperatures also showed varying fractions of impurity phases with the precipitating agents. The effect of surfactant on BFO nanoparticles shows reduction in crystallite size of 16nm and particle size of $59\pm 15\text{nm}$ which further altered the magnetic nature of BFO nanoparticles from antiferromagnetic to a weak ferromagnetic. Further we also studied the effect of template and sol-gel processing conditions on BFO Nanofoams synthesized by sol-gel method. Resultant material was single phase BFO along with minor impurities. We found that there is no change in the crystallite size for BFO from 0.16M to 1M of metal ion concentrations, but primary particles have plate like morphology rather than rhombohedral morphology. Also, there is a change in porosity i.e. porosity decreases from 0.16M to 1M. Therefore the template is playing a role in crystallization process of the material when the concentration of the metal ion is high. Hence it is necessary to know the effect of the above processing conditions in the formation of pure phase BFO.

Nomenclature

BFO (BiFeO_3) - Bismuth ferrite

NaOH - Sodium hydroxide

NH_4OH - Ammonium hydroxide

TMAOH - Tetra methyl ammonium hydroxide

CTAB - Cetyltrimethylammonium bromide

KOH – Potassium hydroxide

LiOH – Lithium hydroxide

PPMS – Physical property measurement system

T_N – Neel transition temperature

T_C – Curie temperature

XRD - X-ray diffraction

FESEM – Field emission scanning electron microscope

TEM – Transmission electron microscope

Oe – Oersted

NCA - Nano channel alumina

AAO - Anodic aluminum oxide

ZFC – Zero field cooling

FC – Field cooling

M-H – Magnetization versus Magnetic field

M-T - Magnetization versus Temperature

FP – Filter paper

FM – Ferromagnetic

T_B - Blocking temperature

Contents

Declaration.....	ii
Approval Sheet.....	iii
Acknowledgements.....	iv
Abstract.....	vi
Nomenclature	vii
1 Introduction	1-6
1.1 Multiferroics.....	1
1.2 Classification of multiferroics	2-4
1.3 Introduction of BiFeO ₃	4-6
2 Literature Review	7
2.1 Literature review on chemical synthesis of BFO.....	7-10
2.2. Literature review on Template-assisted synthesis of BFO	10-13
2.3 Objectives	14
3 Experimental details	15-25
3.1 Co-precipitation method.....	15
3.1.1 Synthesis of BFO nanoparticles by using two different precipitating agents such as Ammonium hydroxide and Tetra methyl ammonium hydroxide.....	15-17
3.1.2 Synthesis of BFO nanoparticles at constant pH and constant concentration.....	17
3.2 Surfactant assisted synthesis of BFO nanoparticles via co-precipitation method.....	18-19
3.3 Synthesis of BFO Nanofoams through sol-gel template method.....	20-22
3.4 Characterization techniques.....	22-25
4 Results and discussion of Co-precipitation method using precipitating agents	26-35
4.1: Synthesis of BFO nanoparticles by using NH ₄ OH and TMAOH.....	26

4.1.1:Structural analysis by X-Ray diffraction.....	26-28
4.1.2:Morphological studies.....	29
4.1.3:Magnetic studies.....	29-32
4.1.4:Raman spectroscopy.....	32-33
4.2: Synthesis of BFO nanoparticles at constant pH and constant concentration.....	34
4.2.1: Structural analysis by X-Ray diffraction.....	34-35
5 .Results and discussion of Surfactant assisted synthesis of BFO Nanoparticles via Co-precipitation method.....	36-40
5.1: Surfactant Introduction.....	36
5.2: Structural analysis by X-Ray Diffraction.....	37-38
5.3: Morphological studies.....	38
5.4: Magnetic studies.....	38-40
6. Results and discussion of BFO Nanofoams synthesized by Sol-gel template method.....	41-45
6.1: Structural analysis by X-Ray Diffraction.....	41-42
6.2: Magnetic studies.....	43-44
6.3: Morphological studies.....	45
7. Summary and Conclusions.....	46
References.....	47-49

Chapter 1

Introduction

1.1 Multiferroics:

Existence of more than one ferroic orders namely ferro/anti-ferroelectric, ferro/antiferromagnetic and ferroelastic in the same material is termed as multiferroicity [1]. Multiferroics has attracted researchers for the past few years to understand the fundamental mechanism of magneto electric coupling both in single phase and composite materials. Single phase compounds (BiFeO_3 , BiMnO_3 , YCrO_3 etc.) are rare due to contradiction between conventional mechanisms of ferroelectricity (cation-off centering – requires empty d orbitals of transition element) and ferromagnetism (requires partially filled d-orbitals of transition element) [1]. Ferroelectricity and magnetism coexist in single phase compounds when two different atoms are present in the system; where one atom is responsible to form electrical dipole moments and other carry the magnetic moment. Bismuth ferrite (BiFeO_3) is a well-known single phase compound, where Bi^{3+} ions leads to ferroelectric ordering and Fe^{3+} induces magnetic ordering respectively. Figure 1.1 shows the possible coupling between different order parameters.

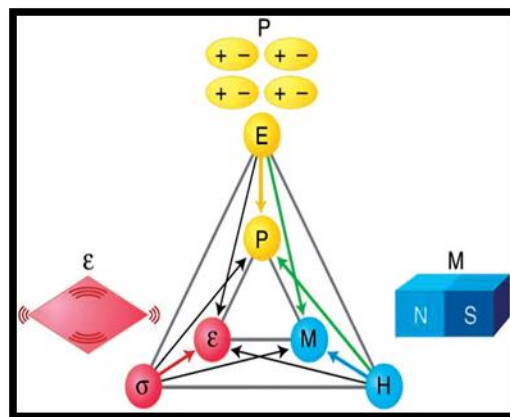


Fig 1.1: Schematic Representation of coupling between different ordered parameters [2]

1.2. Classification of Multiferroics:

Table -1.1: Classification of the Materials based on the mechanism of ferroelectricity [3]

Multiferroics	Mechanism of inversion symmetry breaking	Materials
Type-I	Polarization of $6s^2$ lone pair Geometrically driven ferroelectricity Charge ordered(CO) insulators	E.g. BiFeO_3 or BiMnO_3 E.g. YMnO_3 E.g. $\text{LuFe}_2\text{O}_4, \text{Fe}_3\text{O}_4$
Type-II	Magnetic ordering	E.g. TbMnO_3

Multiferroics can be classified into 2 types

(a): Type-I: Type-I multiferroics are the materials in which the sources of ferroelectricity and magnetism are different and appear quite independent of one another.

(b): Type-II: These are the materials in which ferroelectricity is induced by the magnetism.

Ferroelectricity due to lone pair of electrons:

In materials like BiFeO_3 , BiMnO_3 etc., Bi^{3+} plays a major role in the origin of ferroelectricity. Bi^{3+} contains a stereo chemically active outer $6s^2$ lone pair of electrons. The existence of $6s^2$ (lone pair) favours in breaking the inversion symmetry by driving Bi^{+3} towards oxygen and which results in ferroelectricity.

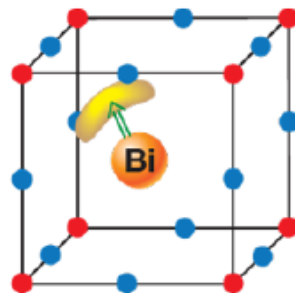


Fig 1.2: Origin of polarization in BiFeO_3 [4]

Geometrically driven ferroelectricity:

In materials such as YMnO_3 , ferroelectricity occurs due to tilting of the rigid MnO_5 trigonal prism. Such tilting results in loss of inversion symmetry and thus leads to ferroelectricity.

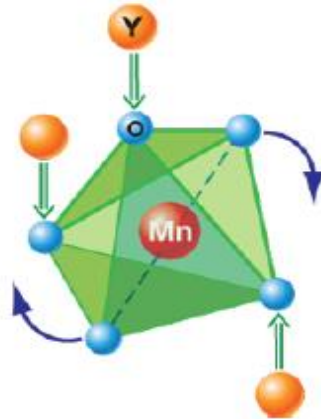


Fig 1.3: Origin of polarization in YMnO_3 [4]

Ferroelectricity due to charge ordering: This type of ferroelectricity is generally observed in transition metal ions with different valence (charge).

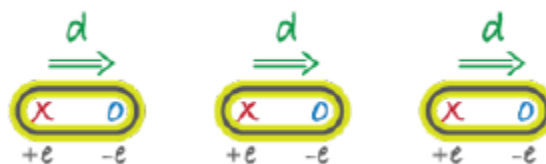


Fig 1.4: Ferroelectricity due to charge ordering [4]

E.g. Charge ordering (CO) in magnetite (Fe_3O_4): The crystal structure of Fe_3O_4 is inverse spinel structure with two distinct iron positions. The iron B sites contain two-third of the iron ions, with equal number of Fe^{3+} and Fe^{2+} . These are present inside oxygen octahedral. The iron A sites contain the other one-third of the Fe ions and are not considered for the charge ordering. The Verwey metal-insulator transition occurs at $T_{12}=120\text{K}$ is related to charge ordering of two types of charges with the alternation of the formal Fe^{2+} and Fe^{3+} valence states. Beside this site centered CO, there is also a strong modulation of Fe-Fe distances which results in polarization. Hence the coexistence of bond-centered and charge-centered charge ordering is the mechanism for ferroelectricity in magnetite [5].

1.2(b) **Type-II:** E.g. TbMnO_3

The magnetic structure of TbMnO_3 is the result of the competition between ferromagnetic (FM) and the antiferromagnetic (AFM) interactions. This competition arises as the Mn-O-Mn bond angle gives rise to the intermediate interactions between anti-ferromagnetic 180° superexchange and

ferromagnetic 90° superexchange. At temperature below $T_{N1}=40\text{K}$ magnetic structure exits in anti-ferromagnetic sinusoidal spin density wave (i.e. all the spins point in one direction) and, a transition to a non-collinear cycloid spin ordering occurs below $T_{N2}=27\text{K}$. This cycloid spin structure breaks the inversion symmetry and allows polarization perpendicular to both the wave vector and the spin rotation axis of cycloid [6]. The plane of a magnetic cycloid rotate by 90° if a magnetic field is applied, then the polarization \mathbf{P} also rotates.

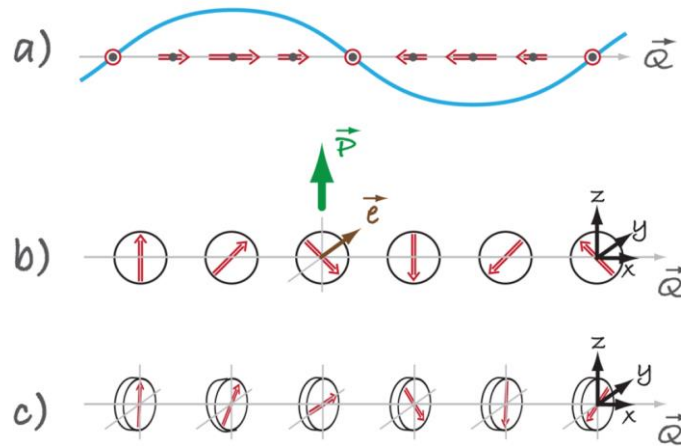


Fig 1.5(a) Sinusoidal spin density wave structure and (b) cycloid spin structure of TbMnO₃[4]

1.3. Bismuth ferrite (BiFeO₃)

Among the single phase multiferroics systems Bismuth ferrite [BiFeO₃ (BFO)] is an extensively studied compound due to its high ferroelectric Curie temperature ($T_C = 1103\text{ K}$) and antiferromagnetic Neel temperature ($T_N = 643\text{ K}$). The presence of high temperature phase transitions makes it useful in novel device applications such as data storage, sensors, spintronic devices etc. [7]. The crystal structure of BFO is distorted rhombohedral perovskite with R3c space group symmetry. The schematic of BFO unit cell is shown in figure 1.6, where, Bi^{3+} occupies corners of the unit cell, Fe^{3+} occupies body-centered position and oxygen occupies face-centered position. The lattice parameters BFO are: $a_r=3.965\text{ \AA}$, $\alpha_r= 89.45^\circ$. The unit cell is also described in a hexagonal system with $a=b=5.58\text{ \AA}$ and $C=13.90\text{ \AA}$ [8].

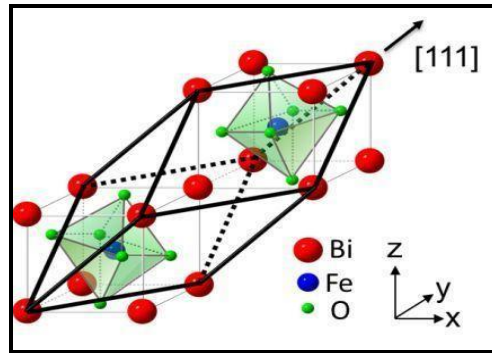


Fig 1.6: Crystal structure of BiFeO₃[9]

Ferroelectricity in BFO is induced by Bi³⁺. Bi³⁺ contains a stereo chemically active outer 6s² lone pair of electrons. The existence of 6s²(lone pair) favour in breaking the inversion symmetry by driving Bi³⁺ towards oxygen which is shown in the figure 1.2 and anti-ferromagnetism is induced by Fe³⁺.

There are several reports which explored the physical properties of BFO both in bulk and thin film form. Effect of elemental substitution in bulk BFO and effect of anisotropy on epitaxial thin films of BFO has been studied to improve its electrical and magnetic properties. BFO shows G-Type anti-ferromagnetic ordering (i.e. Magnetic moments of nearest neighbour Fe³⁺ are aligned antiparallel to each other). This G-type antiferromagnetic structure is modulated to a spiral spin structure, which has a long period of $\lambda = 64\text{nm}$ [10].

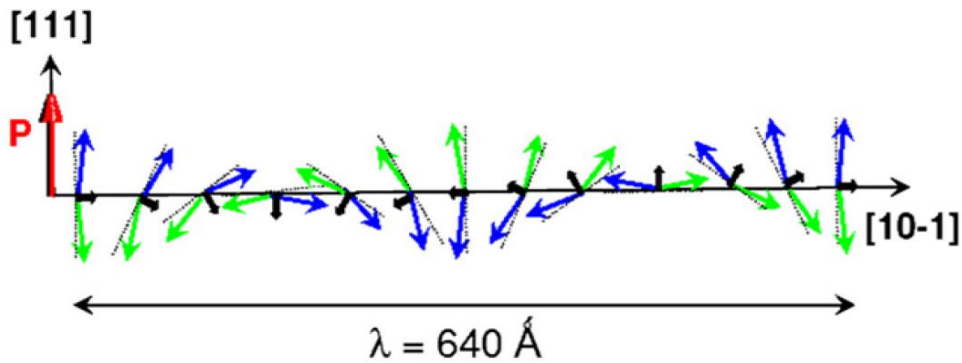


Fig 1.7: Schematic representation of BiFeO₃ cycloid spin structure [10].

Whereas BFO Nanoparticles (of particle size less than 64nm) shows weak ferromagnetic nature because of Dzyaloshinskii-Moriya interaction. Hence there will be some net magnetic moment.

Recent research has focused more on synthesizing the nanostructures of BFO such as nanoparticles; nanorods etc. with reference to their size dependent properties. Generally BFO nanoparticles can be synthesized using traditional solid state method and wet chemical method. The

main aim for all the synthesis processes is to get single phase BFO with high purity at low temperatures and also should be a simple process to make it cost effective for various industrial applications [11].

Solid state method [12] requires high temperature to form the required phase. This high thermal energy helps to overcome the diffusion barrier and allows the ions to migrate through the rigid solid lattice. It often requires heating for several days. In order to prevent these difficulties, wet chemical routes are used.

Wet chemical route includes sol-gel [13], Hydrothermal [14], combustion [15], co-precipitation [16] processes etc. Sol-gel and combustion processes may lead to complex solutions and toxic reactions because of chemical nature of the precursors used in the synthesis. Hydrothermal method requires high pressure and therefore complex equipment is needed to insure the safety during hydrothermal reactions.

In general co-precipitation method is a cheap and simple method. In this process the metal salts are co-precipitated as hydroxides, carbonates, oxalates, formates or citrates [17]. These precipitates are calcined at appropriate temperatures to yield the final powder. In order to achieve high homogeneity, the solubility products of the metal cations must be closer. Homogeneity can be achieved by controlling the synthesis parameters such as concentration, temperature, pH, and mode of addition of the precipitating agent. Co-precipitation results in atomic scale mixing and hence requires lower synthesizing temperature than the above mentioned methods. This leads to smaller particle size in the resulting oxide powders. Further control over particle size and shape can be achieved through use of surface active agents or surfactants.

Chapter-2

Literature Review

Synthesis of single phase BFO is the most important part of this research work. It is difficult to synthesize phase pure BFO. The impurities may arise from three different causes [18]

- ✓ The evaporation of Bi component occurs during its synthesis, because of the low decomposition temperature of bismuth salts; thus Bi_2O_3 component appears again in the final product as an impurity.
- ✓ The chemical valence of Fe ion varies in an oxygen-deficient atmosphere; the charge defects with respect to Fe^{2+} ions produced in the synthesis are usually related to the large leakage current in BiFeO_3 and
- ✓ The synthesis area of single-phase BFO in the phase diagram of Bi_2O_3 – Fe_2O_3 is very narrow.

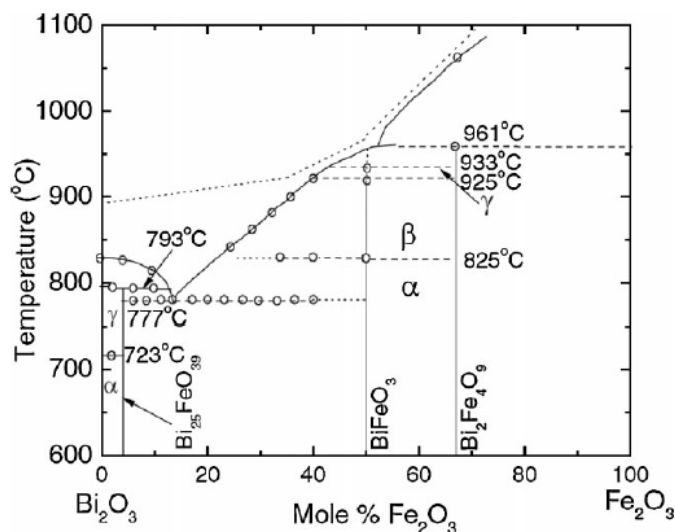


Fig 2.1: Phase diagram of BiFeO_3 [19]

From thermodynamics point of view, two kinds of impurities ($\text{Bi}_2\text{Fe}_4\text{O}_9$ and $\text{Bi}_{25}\text{FeO}_{39}$) are the usual substitutions for BiFeO_3 .

In order to synthesize single phase BFO nanoparticles via wet chemical route, the kinetics of phase formation should be known; kinetics of phase formation depends largely on physicochemical nature of precursors and intermediates. Varying synthesis conditions such as pH, precipitating agents, concentration, surfactant etc. can greatly affect homogeneity, reactivity and consequently morphology of the product. Therefore, by tuning the above processing conditions, different particle

sizes and shapes (morphology) can be synthesized which can alter the properties such as magnetic, optical etc. Therefore it is necessary to know the effect of the above processing conditions in the formation of pure phase BFO.

Zhika Liu et.al, [16] synthesized BFO by chemical co-precipitation method using the starting precursors as $\text{Bi}(\text{NO}_3)_3 \cdot 5\text{H}_2\text{O}$ and $\text{Fe}(\text{NO}_3)_3 \cdot 9\text{H}_2\text{O}$ with 1:1 molar ratio dissolved in 2 moles of HNO_3 solution. They used 2M NaOH for precipitation. They have found the diameter of the nanoparticles ranges from 150 to 200nm from TEM.

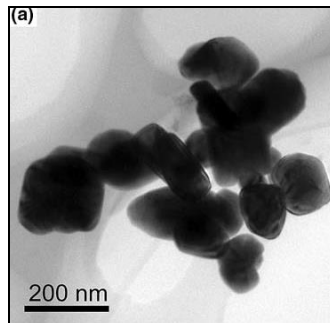


Fig: 2.2.TEM image of BFO Nanoparticles [16].

Later H. Shokrollahi [8] observed a change in the crystallite size of about 36nm by changing the precipitating agent to NH_4OH with pH -9.3 by same co-precipitation method and showed a weak ferromagnetic nature at 300K.

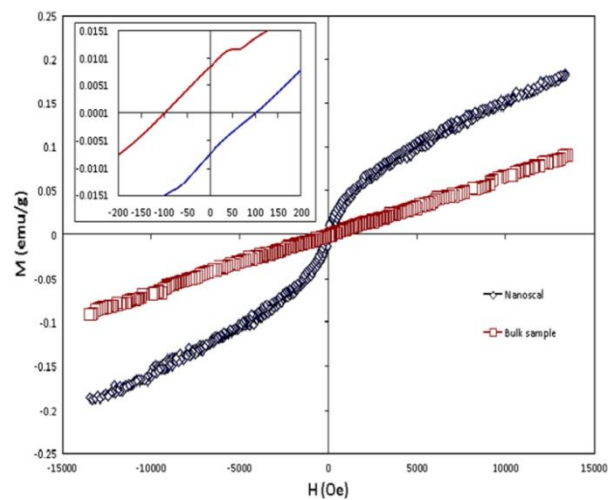
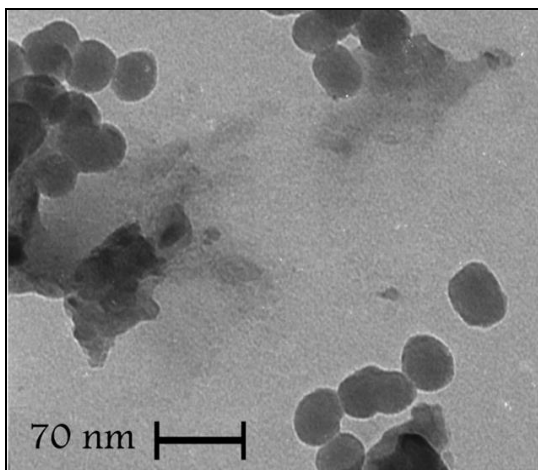


Fig: 2.3 (a)TEM image of BFO Nanoparticles and (b) Hysteresis curve of BFO Nanoparticles at 300K[8].

With the same precipitating agent as NH_4OH , but by changing the conc to 2.5 M. Hua ke et.al [18] synthesized BFO by a modified co-precipitation method. They also reported the synthesis with different pH levels such as 9.3, 9.7, 10 and 11 .They found that at lower pH i.e. 9.3, less impurities

were observed and average crystallite size from XRD, at 550°C was found to be 38 nm. Weak ferromagnetic nature was observed at room temperature.

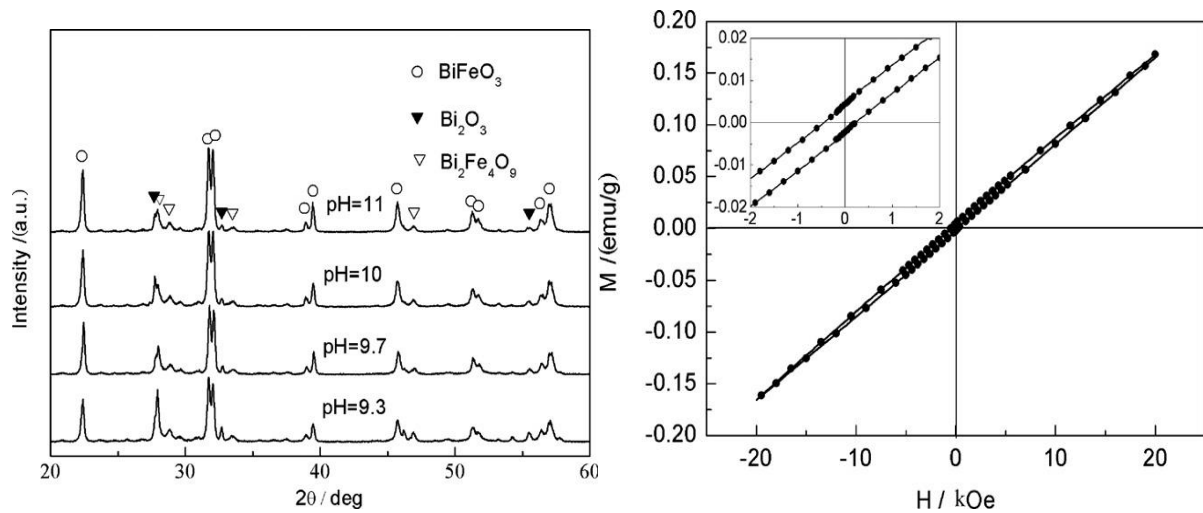


Fig. 2. 4 (a) XRD patterns of the resultant powders prepared at different pH levels (b) M-H loop of BFO Nanoparticles [18].

Mirabbos Hojam Berdriev et.al [20] used various alkaline mineralizers such as KOH, NaOH and LiOH with concentrations ranging from (0.02 M – 0.15M) and synthesized BFO by hydrothermal processing. They used 13.2 M of NH_4OH till PH >10 and they maintained hydrothermal conditions as 180°C for 16 hrs under autogenous pressure. They found that the particle size decreases with decreasing cationic radii of basic mineralizers. The cationic radii of KOH (1.38 Å) > NaOH (1.02 Å) > LiOH (0.75 Å) and the particle sizes are $200 \pm 10 \text{ nm}$ > $120 \pm 5 \text{ nm}$ > $64 \pm 3 \text{ nm}$ respectively.

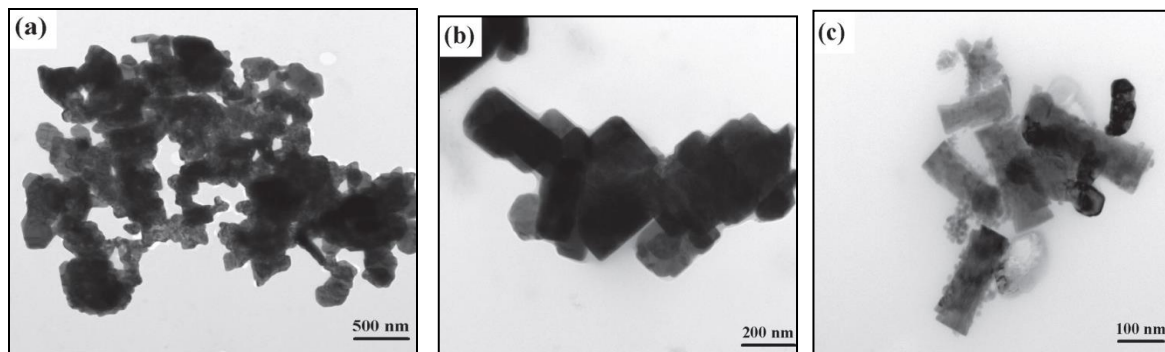


Fig: 2.5(a) TEM image of BFO Nanoparticles synthesized using (a) KOH (b) NaOH (c) LiOH [20].

A.Y Kim et.al,[21] used a surfactant such as cetyltrimethylammonium bromide (CTAB) having concentration of 0.025M along with 8 M KOH and synthesized BFO via hydrothermal process under autogenous pressure at 200°C for 10 hr. Anti-ferromagnetic behaviour was observed at 15 KOe.

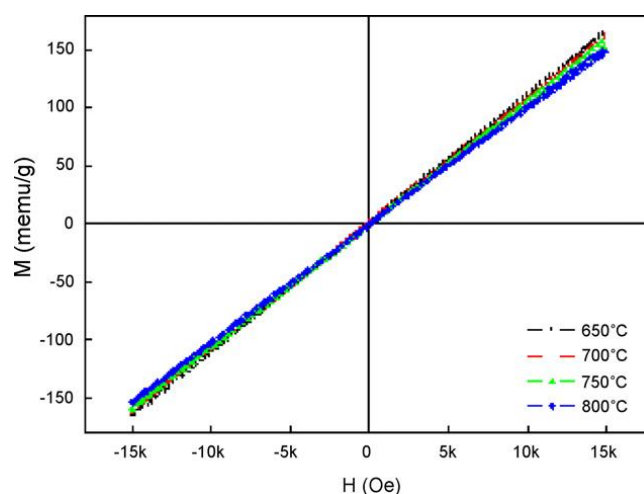


Fig: 2.5. M-H curve of BFO sintered at 650-800°C[21]

Momata Kisku in his thesis[22], also used two different surfactants such as 1.Triton X (non-ionic surfactant) and 2.Ammonium lauryl sulphate (ALS -Anionic surfactant) and synthesized BFO by solution evaporation method and reported that the crystallite size of BFO using ALS at 550 °C was 37.35 nm and while using Triton-X was 62.86 nm.

2.2 Literature review on Template-assisted synthesis of BFO:

Templating is commonly used for the controlled fabrication of nanostructures such as nanorods, nanowires and nanotubes of materials such as polymers, metals, semiconductors and oxides. Generally, ordered structure with desired properties can be obtained by using templating techniques. The general synthesis procedure involves: first a template is filled or covered with a soft precursor material to bring the material into desired form and then through a chemical reaction or physical process the products are formed within the template. Later the template is removed to obtain the desired product [23]

In addition to the desired pore, size, size distribution, morphology, template materials must meet certain requirements such as

- a. Compatible with the processing conditions
- b. Chemically inert during the synthesis
- c. Easy release of the template.

Jie Wei et al [24] synthesized BFO nanotubes by sol-gel method using porous nanochannel alumina (NCA) template. Citric acid ($C_6O_7H_8$) was used as a complexing agent (final concentration of

0.01M). The pH was maintained neutral using ammonia and urea of ratio (1:20) and observed a weak ferromagnetism at room temperature.

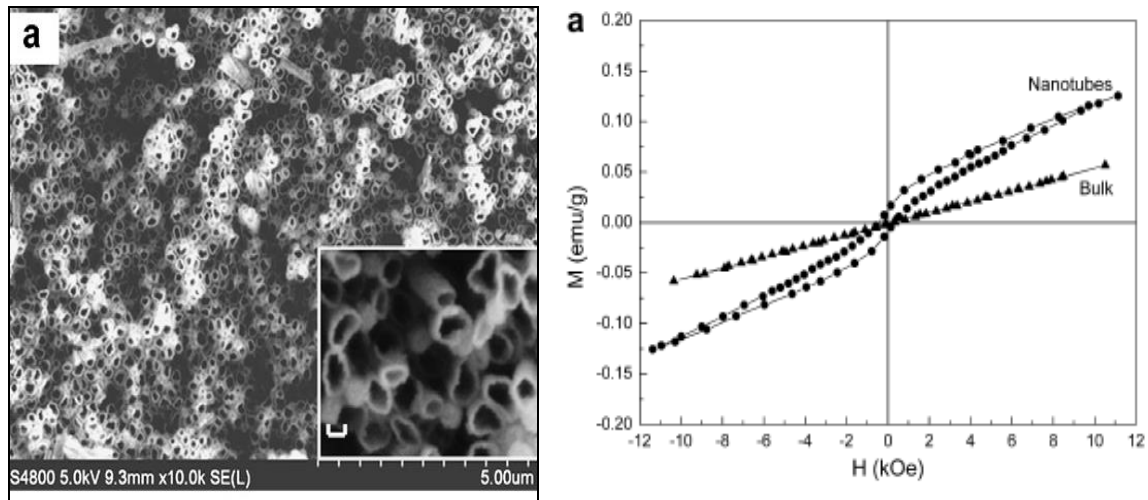


Fig 2.7. (a) SEM image of BFO Nanotube array (b) M–H hysteresis loop for the BFO nanotubes measured at room temperature. [24]

X.Y.Zhang et al [25] also synthesized BFO nanotube with a diameter of about 250nm and length of about 6 μ m by sol-gel method using nanochannel alumina(NCA) template and 2-methoxy ethanol (C₃H₈O₂) as a complexing agent (final concentration of 0.3M)

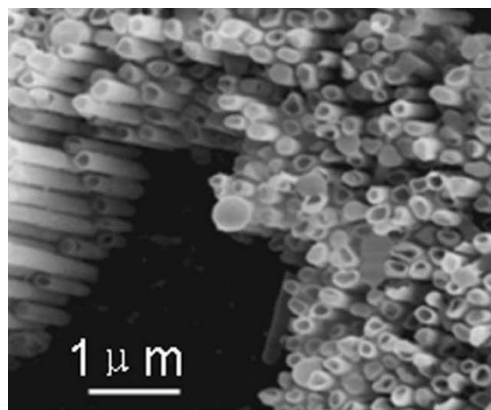


Fig: 2.8: SEM image of BFO nanotube array [25]

Later L.A.S de Oliveira et al[26],observed weak ferromagnetic nature by using Anodic aluminum oxide (AAO) membrane as template where oxalic acid (0.2 M) was used as a complexing agent.

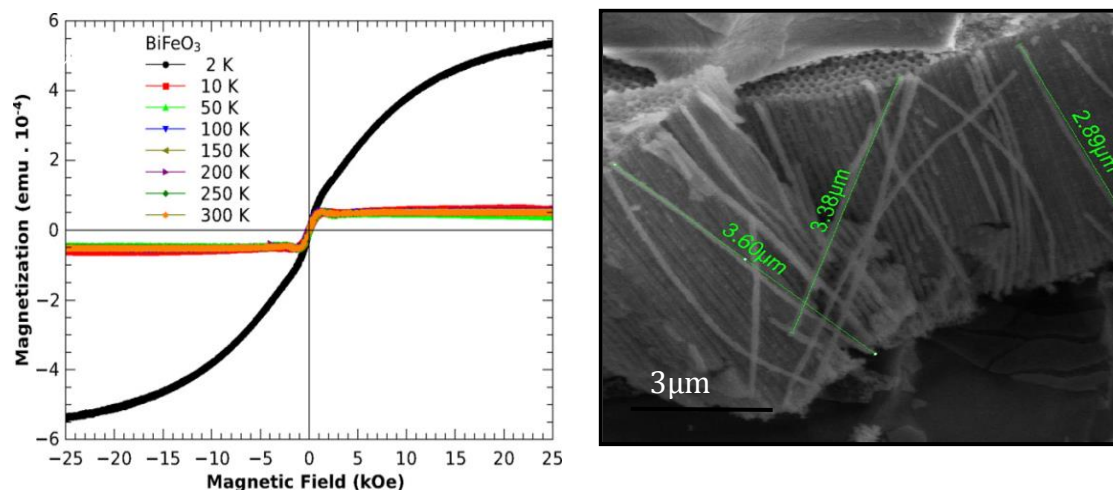


Fig: 2.9 (a) M–H hysteresis loop for the BFO nanotubes measured at different temperatures and (b) SEM image of BFO nanotubes [26].

The below table shows the summarized form of all synthesis procedures which are discussed in the above literature.

Table-2.1: Summary of all the above synthesis processes

Synthesis process	Precipitating /Complexing agents	Reaction conditions	Crystallite/particle size(nm)	Magnetic properties	References
Co-precipitation	NaOH	2M conc	150-200(TEM)	-	[16]
Co-precipitation	NH ₄ OH	pH -9.3	36(XRD)	Weak ferromagnetic nature	[8]
Co-precipitation	NH ₄ OH	pH-9.3, 9.7, 10 and 11	38(XRD) at pH -9.3	Weak ferromagnetic nature	[18]
Hydrothermal	KOH, NaOH and LiOH	(0.02M–0.15 M)	200±10(KOH) >120±5(NaOH)>64 ±3(LiOH)(XRD).	-	[20]
Hydrothermal	KOH and CTAB	8M and 0.025 M	650 °C-5.5 μm 700 °C-11.9 μm	Anti-ferromagnetic	[21]

			800°C-10.3 μm 850°C-68μm (SEM)	nature	
Autocombustion	Glycine Triton X and ALS	0.1moles 0.05moles 0.05moles	37.35 62.8(XRD)	-	[22]
Sol-gel template method	citric acid + urea+ NCA template	0.01M + pH- 7	diameter of about 180nm. The thickness of wall of about 20nm. (TEM)	Weak ferromagnetic nature	[24]
Sol-gel template method	2-methoxy ethanol+ NCA template	0.3M+ pH=1-2	the average wall thickness of nanotubes is about 20 nm(TEM)	-	[25]
Sol-gel template method	Oxalic acid+ AAO membrane	0.2M	diameters of about 65 nm and wall thickness of about 16 nm.(SEM)	Weak ferromagnetic nature	[26]

From the above literature review it was found that the precipitating agents with different reaction conditions, such as effect of pH, concentration, surfactant etc. plays an important role in controlling the particle size and shape (morphology) etc. of pure phase BFO nanoparticles and which finally affects the properties such as magnetic, optical etc.

2.3 Objectives:

The work has been done with the following objectives

1. To control the crystallite size of bismuth ferrite (BFO) nanoparticles by using two different precipitating agents such as ammonium hydroxide(NH_4OH) and tetra methyl ammonium hydroxide(TMAOH) at constant pH and constant concentration.
2. To study the role of surfactant (cetyltrimethylammoniumbromide) in controlling the crystallite size of bismuth ferrite and the effect of size dependence magnetic properties of bismuth ferrite nanoparticles.
3. Synthesis of BFO Nanofoams using Whatman filter paper by sol-gel method and study the effect of template and sol-gel processing conditions on resultant BFO nanostructures.

Chapter 3

Experimental details

The objective of this work is mainly focused on the synthesis of phase pure BiFeO₃ via wet chemical method. We synthesized BFO through co-precipitation method and sol-gel method. This chapter describes the synthesis procedures and also the basic principles of X-ray diffraction (XRD), Raman spectroscopy, scanning electron microscopy (SEM) and Vibrating sample magnetometer (VSM).

3.1. Co-precipitation method:

3.1.1: Synthesis of BFO nanoparticles by using two different precipitating agents such as Ammonium hydroxide and Tetra methyl ammonium hydroxide at constant pH:

Chemicals: Bismuth nitrate penta hydrate [Bi (NO₃)₃.5H₂O, sigma Aldrich >98.0%], Iron (III) nitrate nonahydrate [Fe (NO₃)₃.9H₂O, sigma Aldrich >98.0%], Tetra methyl ammonium hydroxide (sigma Aldrich, 25 wt %), Ammonium hydroxide (sigma Aldrich, 28-30 wt %) and Nitric acid (HNO₃, SDFCL, 69-72%), was used for the synthesis of BFO nanoparticles.

Procedure: Bismuth nitrate penta hydrate and Iron nitrate nonahydrate were used as initial precursors. 0.025moles of Bi (NO₃)₃.5H₂O was dissolved in 10 ml of dilute nitric acid and 0.025 moles of Fe (NO₃)₃.9H₂O was dissolved in 10 ml of deionized water. These solutions were mixed to obtain a uniform transparent mixed solution. This mixture was added to the precipitating agents such as NH₄OH and TMAOH separately with constant stirring. Constant pH of 14 was maintained in this process. So 5.92M solution of NH₄OH and 2M solution of TMAOH was used in order to maintain the constant pH as 14. The solution thus obtained was brown in colour and it was washed successively with deionized water till pH-7 was achieved. After washing, the precipitate was dried in hot air oven at 60°C. Dried precipitate was ground to fine powder using agate mortar and pestle.

The below fig 3.1 shows the flow chat of the synthesis procedure.

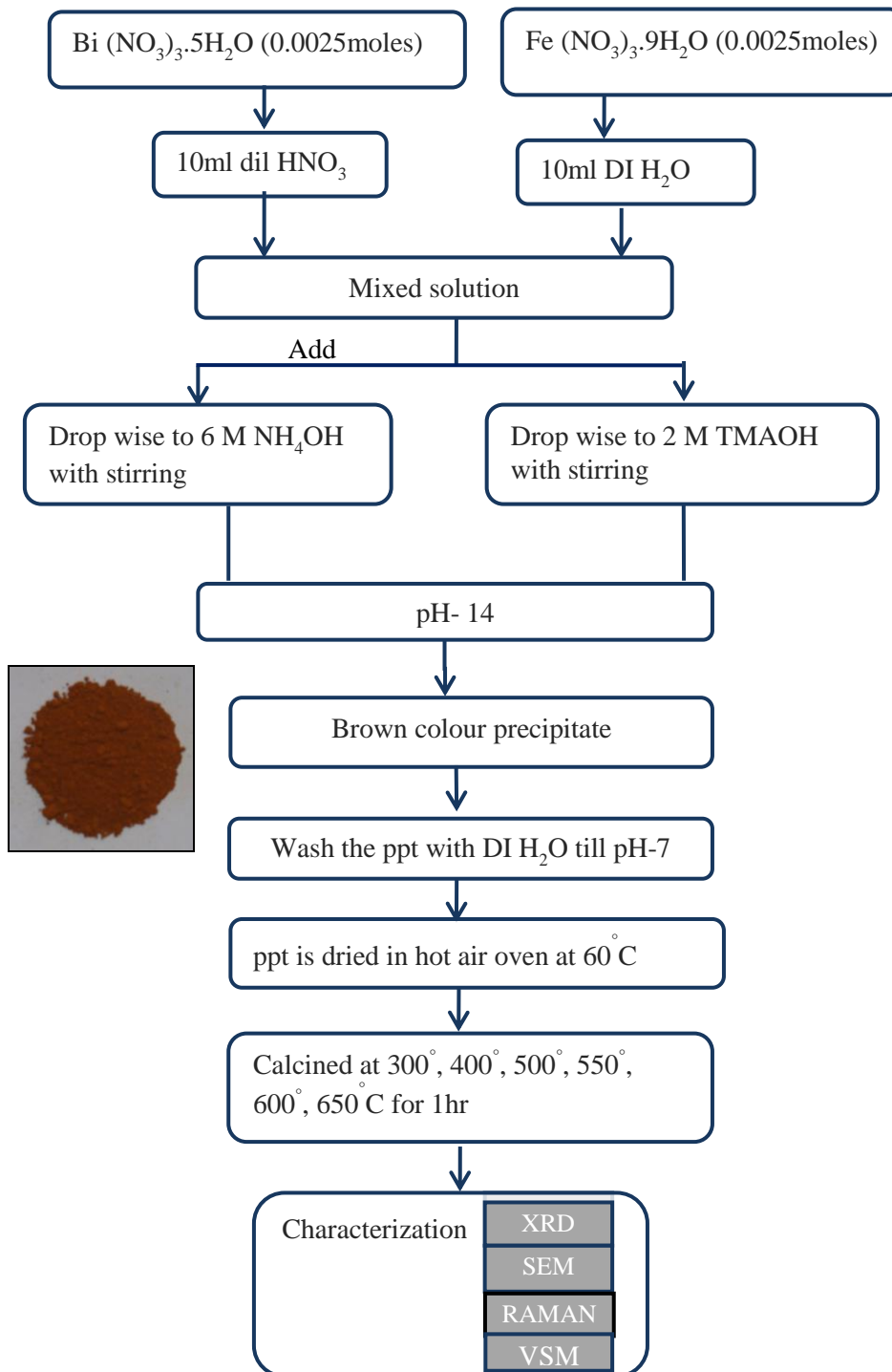


Fig 3.1: Synthesis procedure of BFO

Calcination:

Calcination is a heat treatment process in solids in order to bring about thermal decomposition, phase transition or removal of a volatile fraction. Calcination process normally takes place at temperature below the melting point among the precursors [12].

The above resultant powder were calcined at different temperatures such as 300 °C, 400 °C, 500 °C, 550 °C, 600 °C and 650 °C for 1 hour with a step size of 5 °C/ min in a muffle furnace, in order to determine the phase evolution. Phase purity was characterized by X-ray diffraction. . This powder was further analyzed by SEM and VSM.

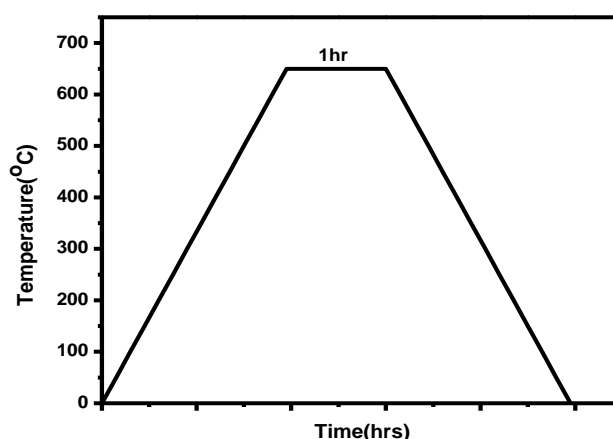


Fig 3.2: Calcination profile of BFO at 650°C.

3.1.2: Synthesis of BFO nanoparticles at constant pH and constant concentration

The above synthesis procedure was repeated at constant concentration of 2M using the three precipitating agents such as NaOH, NH₄OH and TMAOH. pH -12 was maintained in all the three cases. The powers obtained were calcined at 550 °C for 1hr with a step size of 5 °C/ min in a muffle furnace.

Calcination profile:

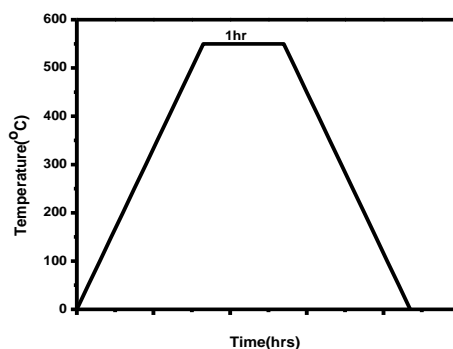


Fig 3.2: Calcination profile of BFO at 550 °C.

3.2. Surfactant assisted synthesis of BFO nanoparticles via Co-precipitation method:

Chemicals: Bismuth chloride (BiCl_3 , sigma aldrich >98%), Iron (III) nitrate nonahydrate [$\text{Fe}(\text{NO}_3)_3 \cdot 9\text{H}_2\text{O}$, sigma aldrich, >98.0%], Sodium hydroxide (NaOH , SDFCL INDIA, 96%), Cetyltri methylammoniumbromide (CTAB, sigma Aldrich, 99 %.), Hydrochloric acid (HCl SDFCL, 35-38%), Methanol (CH_3OH , VETEC, 99%).

Procedure: BiCl_3 , $\text{Fe}(\text{NO}_3)_3 \cdot 9\text{H}_2\text{O}$ and CTAB were used as precursors. 0.0025 moles of BiCl_3 were dissolved in 8 ml of HCl and 0.0025 moles of $\text{Fe}(\text{NO}_3)_3 \cdot 9\text{H}_2\text{O}$ were dissolved in 3.2 ml of methanol so as to make up the final volume of 4 ml. Both the solutions were mixed and to that solution, 0.005 moles of CTAB which was dissolved in 10 ml of methanol was added. The resultant solution was not clear solution but was yellowish white precipitate. To this precipitate 1 gm of NaOH dissolved in 25 ml of methanol was added drop wise with constant stirring. The solution thus obtained was brown in colour and it was washed successively with deionized water till pH-7. After washing, the precipitate was dried in hot air oven at 60°C . Dried precipitate was ground to fine powder using agate mortar and pestle and calcined at 550°C for 1 hour with a step size of $5^\circ\text{C}/\text{min}$ in a muffle furnace in order to determine the phase. Phase purity was characterized by X-ray diffraction. This powder was further analyzed using SEM and VSM.

Calcination profile:

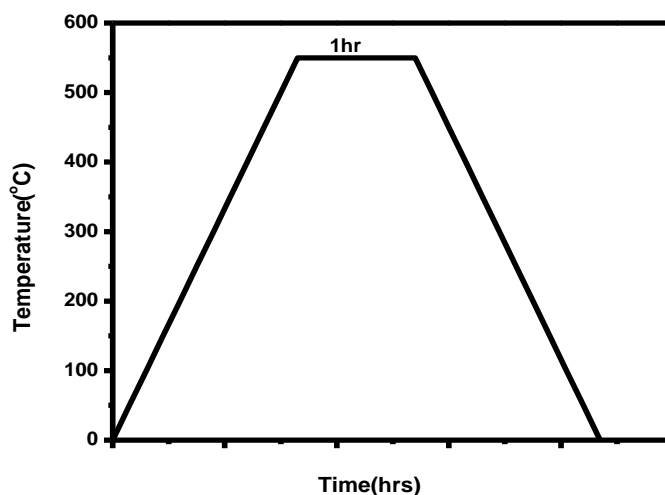


Fig 3.3: Calcination profile of BFO at 550°C .

The flow chart of synthesis procedure is shown in fig: 3.4.

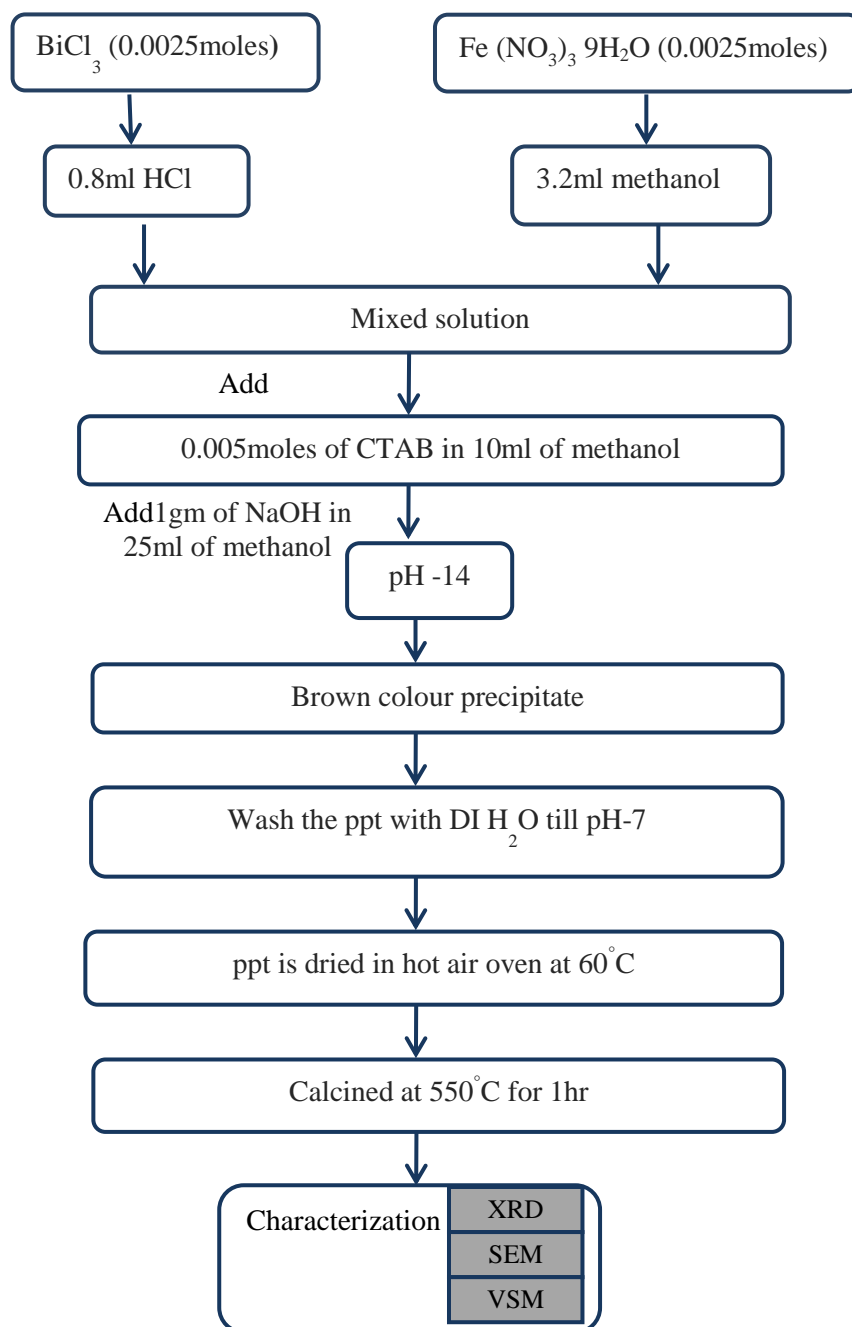


Fig: 3.4. Surfactant assisted synthesis of BFO nanoparticles procedure through co-precipitation method

3.3. Synthesis of BFO Nanofoams through sol gel template method:

Chemicals: Bismuth nitrate penta hydrate [$\text{Bi}(\text{NO}_3)_3 \cdot 5\text{H}_2\text{O}$, sigma Aldrich, >98.0%], Iron (III) nitrite nonahydrate [$\text{Fe}(\text{NO}_3)_3 \cdot 9\text{H}_2\text{O}$, sigma Aldrich, >98.0%], Nitric acid (HNO_3 , SDFCL, 69-72%), Citric acid ($\text{C}_6\text{O}_7\text{H}_8$, SISCO Res.Lab pvt Ltd, INDIA, 99.5%), Whatman filter paper (GE Health care, 50mm dia. UK Ltd).

Procedure: 0.0025 moles of $\text{Bi}(\text{NO}_3)_3 \cdot 5\text{H}_2\text{O}$ were dissolved in 10 ml of dilute nitric acid and 0.0025 moles $\text{Fe}(\text{NO}_3)_3 \cdot 9\text{H}_2\text{O}$ were dissolved in 10 ml of deionized water and both the solutions were mixed to obtain a uniform transparent solution. To that metal solution, 0.005 moles of citric acid which was dissolved in 10 ml of water was added and final solution was stirred for 10-15 min. Thus the final volume used was 30ml. (i.e. 0.16M of total metal ion concentration).

A Whatman filter paper of dimensions 25 x 10 cm were used for this synthesis. The papers were soaked in the above solution for 10 min. The filter paper filled with the solution was dried in hot air oven at 60°C . The dried paper shows conversion of sol to gel and it was further calcined at 650°C for 1 hour. The phase purity was determined by X-ray diffraction. This powder was further analyzed using SEM and VSM. The above procedure was carried out with different final volumes of the solution such as 20ml (0.25M), 10ml (0.5M) and 5ml (1M).

Calcination profile:

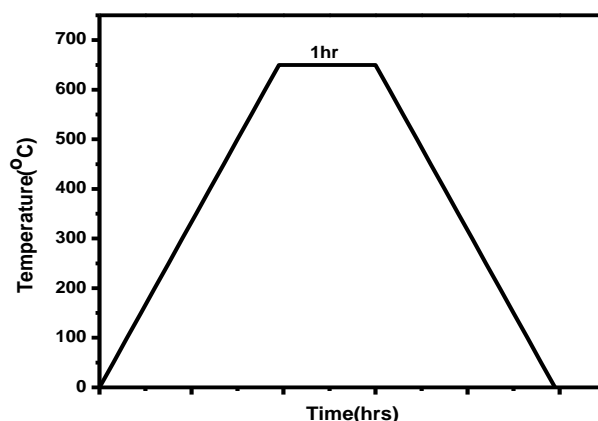


Fig 3.5: Calcination profile of BFO at 650°C .

The flow chart of synthesis procedure is shown in fig: 3.5.

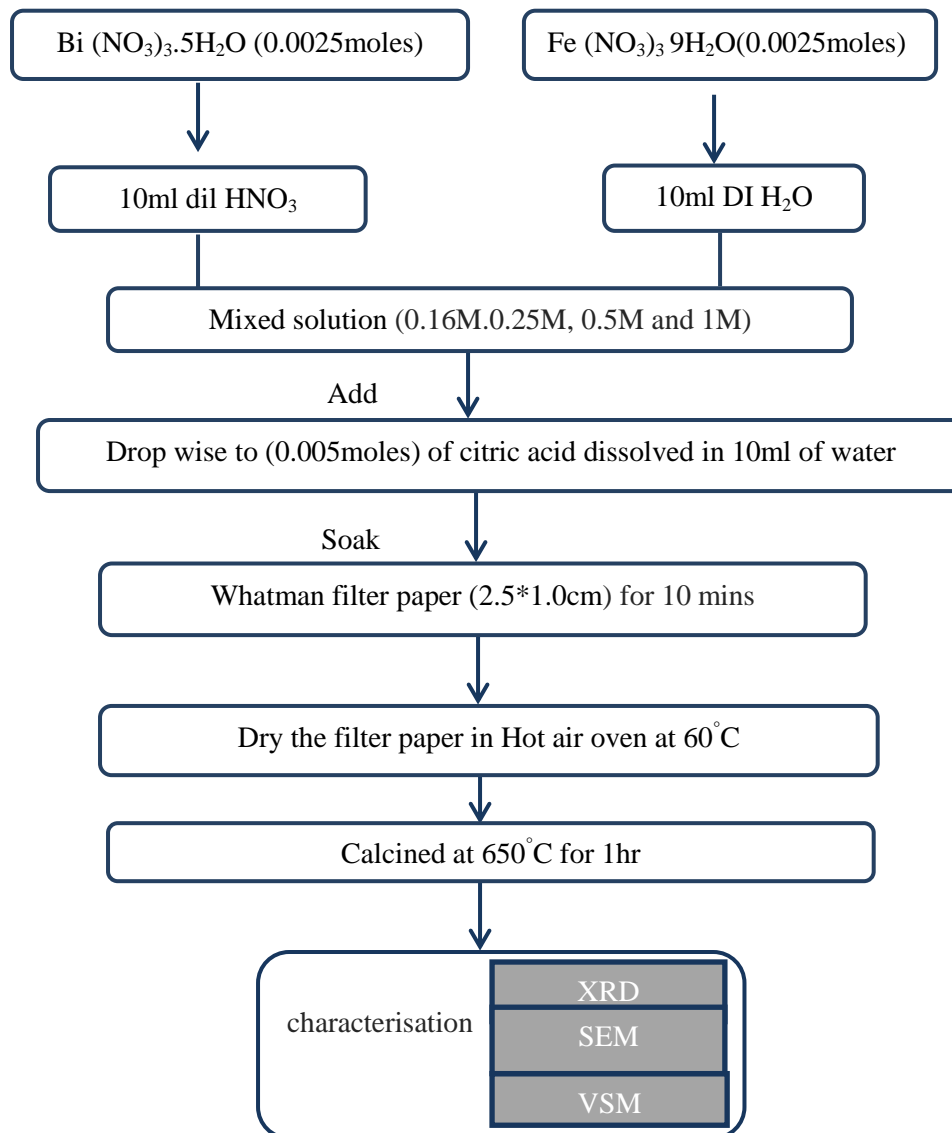
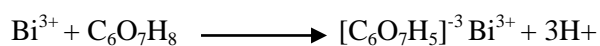
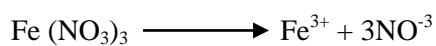
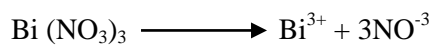
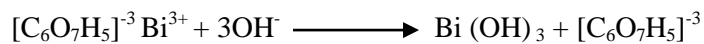


Fig 3.6: Synthesis procedure of BFO Nanofoams synthesized by sol-gel template method.

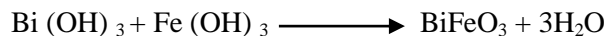
The reactions [27] of sol-gel synthesis of BFO are shown below.



I: Hydrolysis:



II: Condensation:



3.4: Characterization techniques:

3.4.1 X-Ray Diffraction (XRD):

X-rays can be used to study the crystal structures because the interplanar spacing in a crystal lattice is of the same order as that of the wavelength of x-rays. Hence x-ray diffraction technique is used for structural analysis of the material. A collimated beam of X-rays is diffracted by the crystalline phases in the sample according to Bragg's Law i.e. when a crystal is bombarded with x-rays of a fixed wavelength and at certain angles, intense reflected x-rays are produced when the wavelengths of the scattered x-rays interfere constructively. In order for the waves to interfere constructively, the differences in the travel path must be equal to integer multiples of the wavelength which is known as Bragg's Law.

$$n\lambda = 2d\sin\theta \dots\dots\dots(3.4)$$

Where λ = wavelength of the X rays

d = interplanar spacing

n = order of reflection and

θ = angle of diffraction.

The below figure shows the phenomenon of X-ray diffraction.

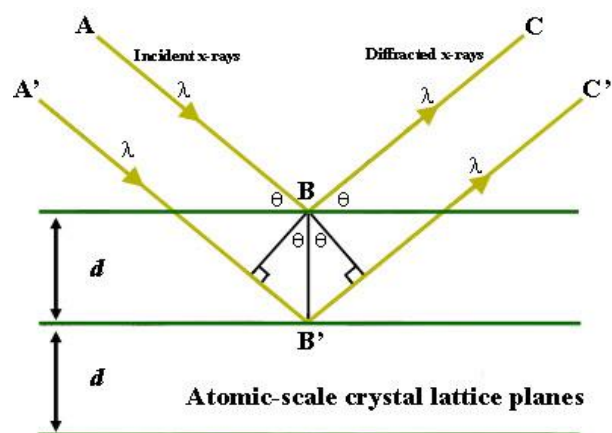


Fig 3.7: Schematic representation of Bragg's law [28]

In the above figure the X-rays are incident on the set of parallel planes ABC and ABC' with an incident angle θ and scattered with the same angle. If these scattered rays forming two parallel planes are in phase, then they give the peak

Phase identification can be done by matching the XRD pattern with reference patterns of pure substances. The reference patterns are known as JCPDS files. It is a collection of single phase X-ray powder diffraction patterns in the form of table of characteristic interplanar spacing and corresponding relative intensities along with crystallographic properties. From this the information of crystal structure, crystallite size, phase purity, lattice parameters etc can be determined.

PAN Alytical expert pro X ray diffractometer with copper $K\alpha$ ($\lambda=1.54\text{\AA}$) radiation was used in the present thesis to investigate phase and crystal structure of the materials.

3.2.2 Scanning electron microscope (SEM):

Morphology and compositional studies was done using Carl Zeiss Super 40 SEM. The electron beam interacts with the material, causing a variety of signals; secondary electrons, backscattered electrons, X-rays, photons, etc. each of which may be used to characterize a material with respect to specific properties. Secondary electrons are used for surface topography whereas backscattered electrons are used for compositional analysis. All the samples were coated with gold sputtering in order to make them conductive [29].

3.2.3 Raman spectroscopy:

Raman Spectroscopy is a vibrational spectroscopy which occurs due to inelastic scattering of light from the substance. When the light source interacts with a molecule, the molecule excites to the virtual energy state where it has short life and comes back to higher or lowers vibrational energy state

by scattering. In this process energy transfer can be done between photon and system. If the scattered photon has more energy than incident photon then it is called as Anti-stokes scattering ($h\nu_0 + h\nu_1$). It has high energy and short wavelength. If the scattered photon has less energy than incident photon then it is called as Stokes scattering ($h\nu_0 - h\nu_1$). It has low energy and long wavelength. Raman spectrum is a plot of intensity of scattering (Raman) as a function of wavenumber [12].

The below figure explains the Raman scattering phenomenon.

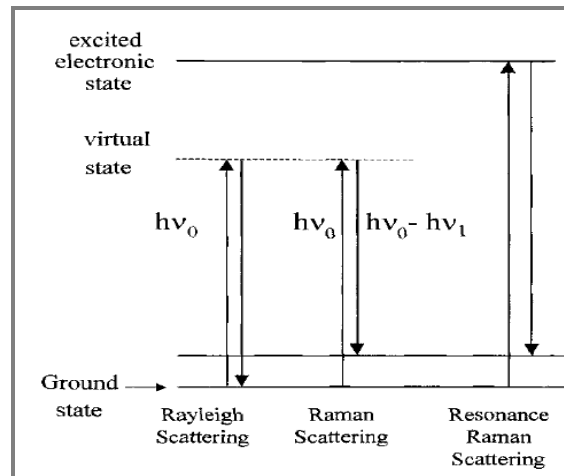


Fig 3.8: Raman scattering phenomenon [12]

Laser Micro Raman spectrometer (Bruker, Senterra) was used in the present thesis to obtain Raman spectrum.

3.2.3 Physical property measurement system (PPMS):

Dynacool from Quantum design PPMS was used in the present thesis to measure magnetic properties of BFO.

Working Principle of VSM:

A vibrating sample magnetometer (VSM) operates on Faraday's Law of Induction, which tells us that a change in magnetic field will produce an electric field. This electric field can be measured and can tell us information about the changing magnetic field. A VSM is used to measure the magnetic behavior of magnetic materials. The sample is kept in a constant magnetic field. If the sample is magnetic, this constant magnetic field will magnetize the sample by aligning the magnetic domains, or the individual magnetic spins, with the field. The stronger the constant field, the larger the magnetization will be. The magnetic dipole moment of the sample will create a magnetic field around the sample, sometimes called as magnetic stray field. As the sample is moved up and down, this magnetic stray field changes as a function of time and can be sensed by a set of pick-up coils. The

alternating magnetic field will cause an electric current in the pick-up coils according to Faraday's Law of Induction. This current will be proportional to the magnetization of the sample. The greater the magnetization, the greater the induced current. The induction current is amplified by a transimpedance amplifier and lock-in amplifier [30].

Chapter-4

Results and discussion:

4.1: Synthesis of BFO nanoparticles by using two different precipitating agents such as Ammonium hydroxide and Tetra methyl ammonium hydroxide.

4.1. 1: Role of precipitating agents in Phase evolution of Bismuth ferrite nanoparticles at constant pH:

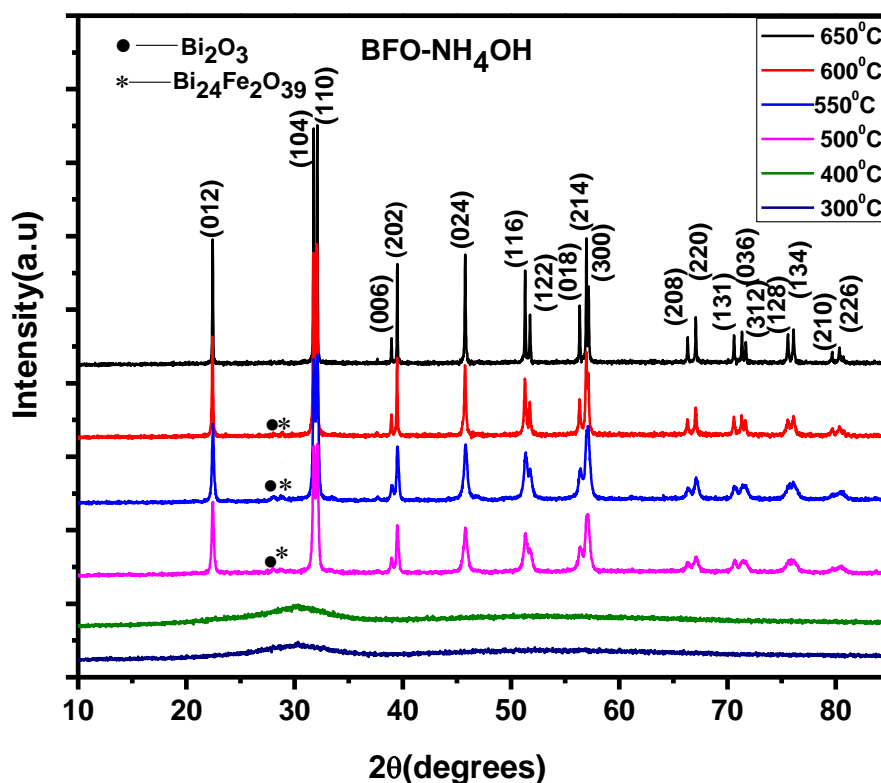


Fig: 4.1 XRD Patterns of bismuth ferrite nanoparticles synthesized using Ammonium hydroxide

Fig 4.1 shows XRD patterns of BFO nanoparticles synthesized using 6M NH₄OH, at constant pH -14 and calcined at different temperatures such as 300°C, 400°C, 500°C, 550°C, 600°C and 650°C. Single phase BFO nanoparticles are obtained at 650°C with reference to the JCPDS NO: 861518. The lattice parameter of (110) is found to be 3.93Å. The crystallite size is calculated using Debye- Scherrer formula.

$$D = 0.94\lambda / \beta \cos\theta \dots \dots \dots [4.1]$$

Where D = crystallite size

λ = wavelength of X-ray radiation (1.54Å)

θ = angle of diffraction

$$\beta = \text{line width} = \sqrt{(\beta_s^2 - \beta_m^2)}$$

and it is found to be 118nm at 650°C

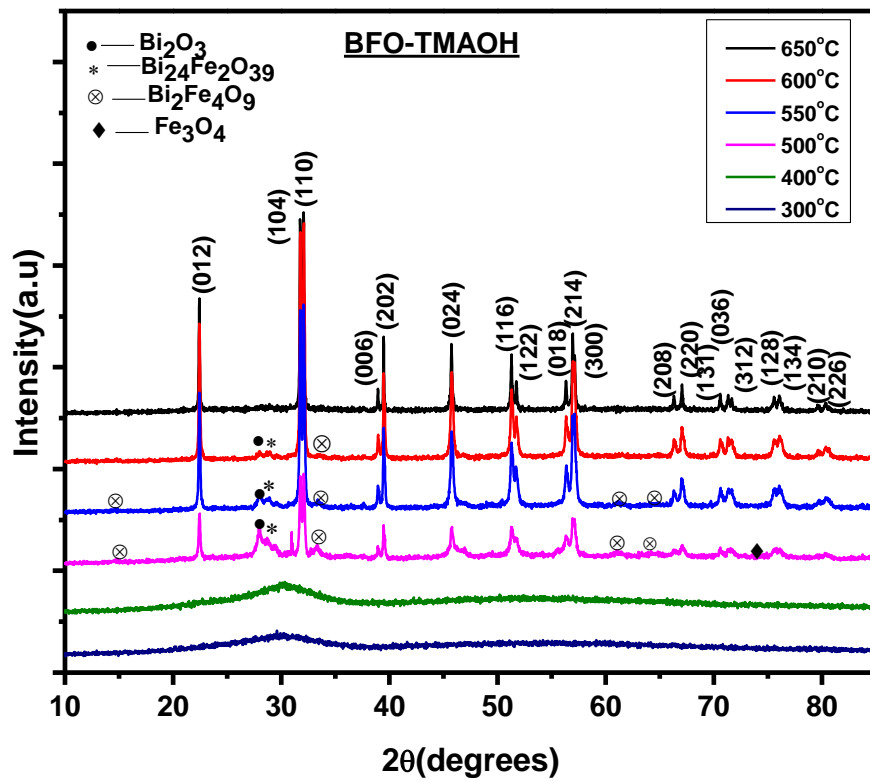


Fig: 4.2 XRD Patterns of bismuth ferrite nanoparticles synthesized by Tetra methyl Ammonium hydroxide (TMAOH).

Fig 4.2 shows XRD patterns of BFO nanoparticles synthesized using 2M TMAOH, at constant pH -14 and calcined at different temperatures such as 300°C, 400°C, 500°C, 550°C, 600°C and 650°C. Single phase BFO nanoparticles is obtained at 650°C with reference to the JCPDS NO: 861518. The lattice parameter of (110) is found to be 3.93Å. The crystallite size calculated from Debye-Scherrer formula is found to be 76nm at 650°C.

Compared to NH_4OH , TMAOH is a strong base. At constant pH -14; TMAOH shows smaller crystallite size (76nm). This is because TMAOH dissociates faster than NH_4OH and releases hydroxyl ions faster. As a result, large number of particles are formed during nucleation and hence growth occurs slowly. In the case of NH_4OH , less number of particles are formed during nucleation as it dissociates slowly when compared to TMAOH and growth occurs faster which results in larger crystallite size (118nm). The cationic radii of $(\text{CH}_3)_4\text{NH}_4^+$ is 2.3\AA [31]. The cationic radii of NH_4^+ is 1.43\AA .

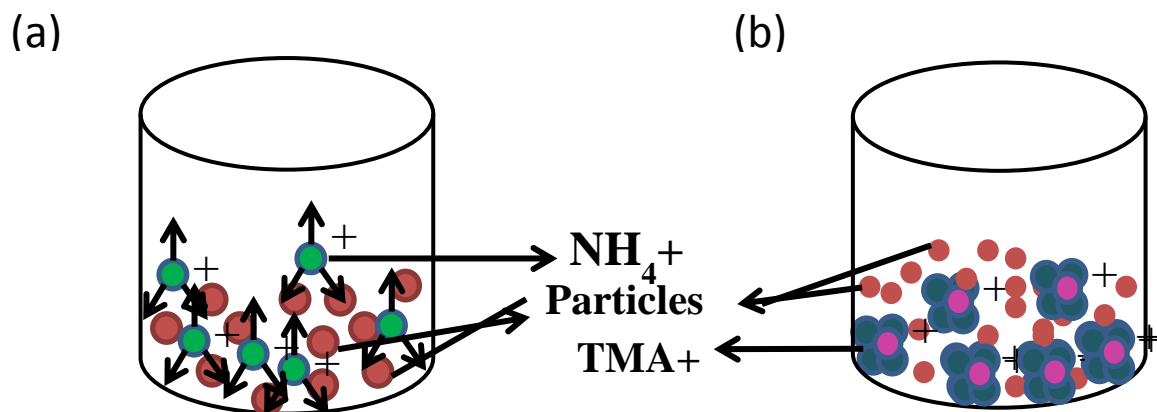


Fig: 4.3.Schematic representation of (a) BFO nanoparticles with NH_4OH and (b) with TMAOH

The structure of TMAOH is given below:

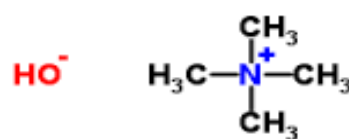


Fig: 4.4.Structure of TMAOH.

This tetra methyl ammonium cation which is a quaternary ammonium ion can also act as a capping agent (surfactant) among the primary particles which is shown in figure 4.3(b) and as a result there is a decrease in crystallite size when compared to NH_4OH .

Varying fractions of impurity phases was also observed with the precipitating agents at lower calcination temperatures and the impurity phases were found to be higher in case of TMAOH

precipitating agent. This is because of uncontrolled precipitation due to faster nucleation. This uncontrolled precipitation makes it inhomogeneous which leads to large amount of impurities.

4.1.2 Morphological studies:

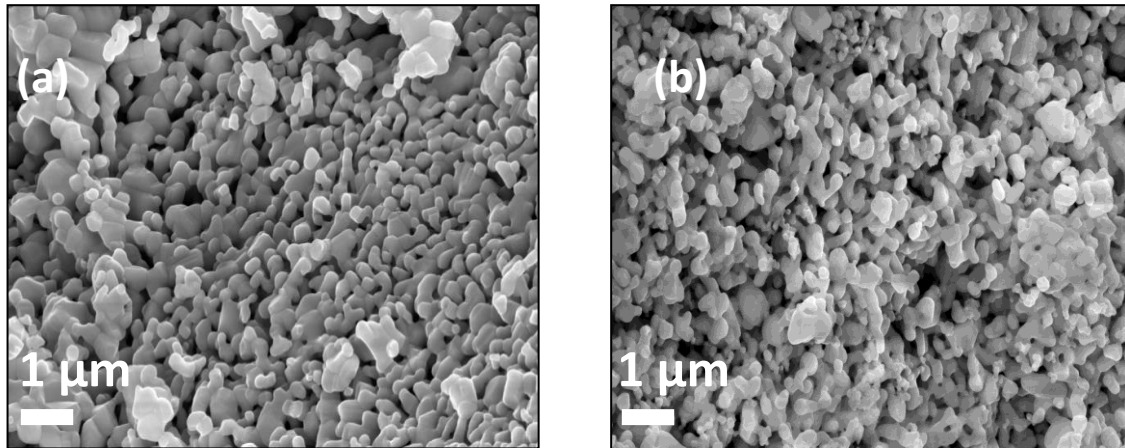


Fig 4.5(a) shows FESEM image of BFO nanoparticles synthesized using NH₄OH and (b) shows FESEM image of BFO nanoparticles synthesized using TMAOH.

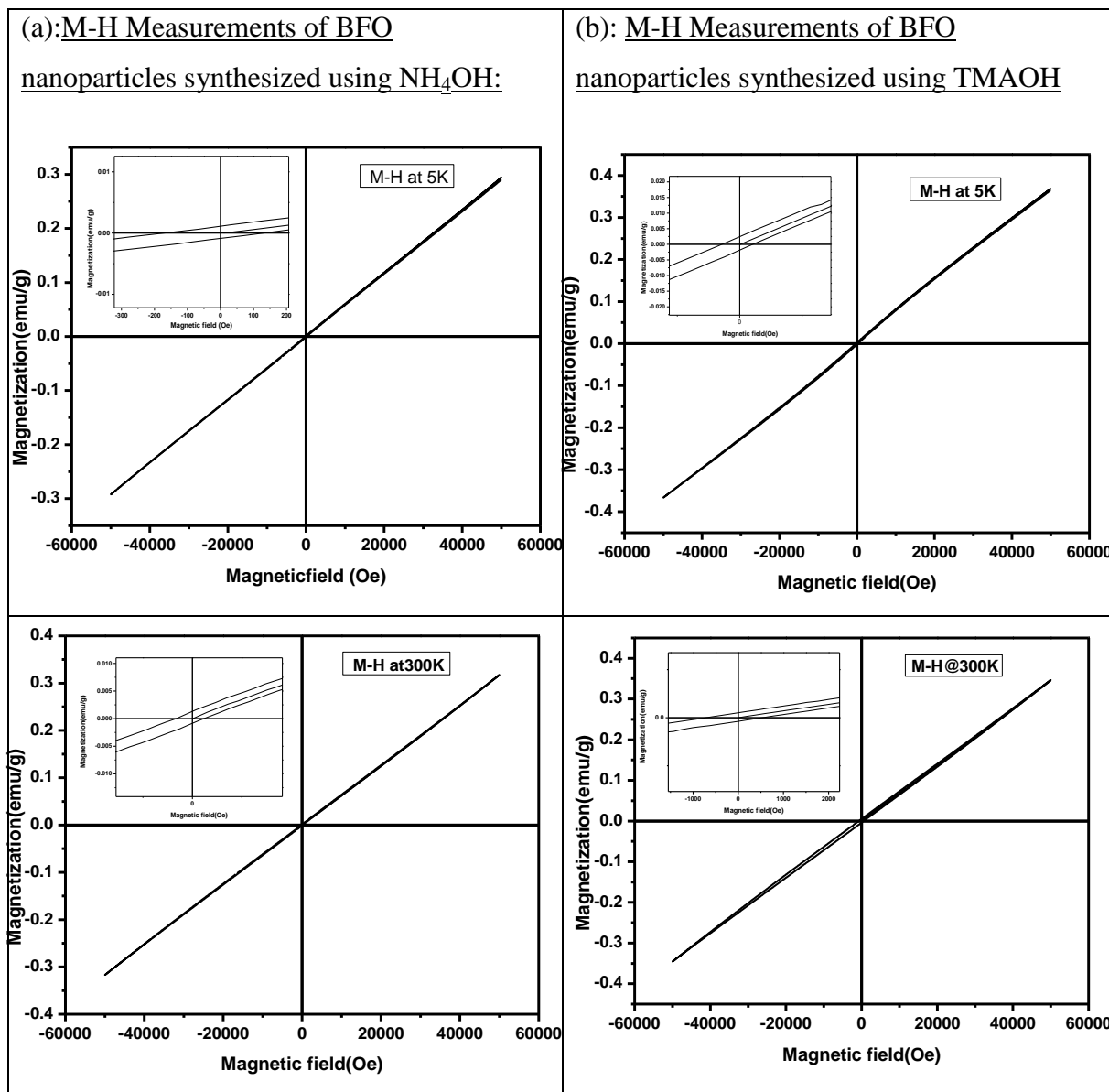
Figure 4.5(a) shows FESEM image of BFO nanoparticles synthesized using NH₄OH precipitating agent and fig 4.5 (b) shows FESEM image of BFO nanoparticles synthesized using TMAOH precipitating agent. It is found that the precipitating agent seems to affect the morphology to some extent. From FESEM image the average particle size of BFO nanoparticles using ammonium hydroxide is found to be $196 \pm 115 \text{ nm}$ and $207 \pm 50 \text{ nm}$ for tetra methyl ammonium hydroxide (particle size is calculated using Image J software). This shows that the precipitating agent TMAOH is effective in controlling the particle sizes than NH₄OH.

4.1.3. Magnetic studies:

Table: 4.1: Values of magnetization and coercivity at 5K and 300K

Precipitating agent	Crystallite size(nm) at 650°C	Remnant magnetization (M _r)(emu/g)		Coercivity (H _c)(Oe)	
		5K	300K	5K	300K
NH ₄ OH	118	0.0013	0.0011	149.9	146.16
TMAOH	76	0.0024	0.0046	253.86	616.91

Table: 4.2: M-H curve of BFO nanoparticles synthesized by (a) NH₄OH and (b) TMAOH.



Magnetic measurements of BFO nanoparticles synthesized by co-precipitation method are performed using PPMS operating in VSM mode. Table: 4.1 shows values of remnant magnetization (which is expressed in emu/g) and coercivity (in Oe) at both 5K and 300K. The values obtained for precipitating agent TMAOH is slightly higher because of its small crystallite size than the NH₄OH. This indicates that the precipitating agent also seems to affect the magnetic properties of BFO nanoparticles.

Magnetic measurements was performed at 5K and 300K .Table 4.2 (a) shows linear M-H curve at both 5K and 300K.A minor slope change in the curve which is shown in figure 4.6, indicates antiferromagnetic behaviour at both 5K and 300K.The coercive fields calculated above after correcting the VSM instrument error (error: $\pm 40\text{Oe}$ to $\pm 60\text{Oe}$) indicates a weak antiferromagnetic behaviour.

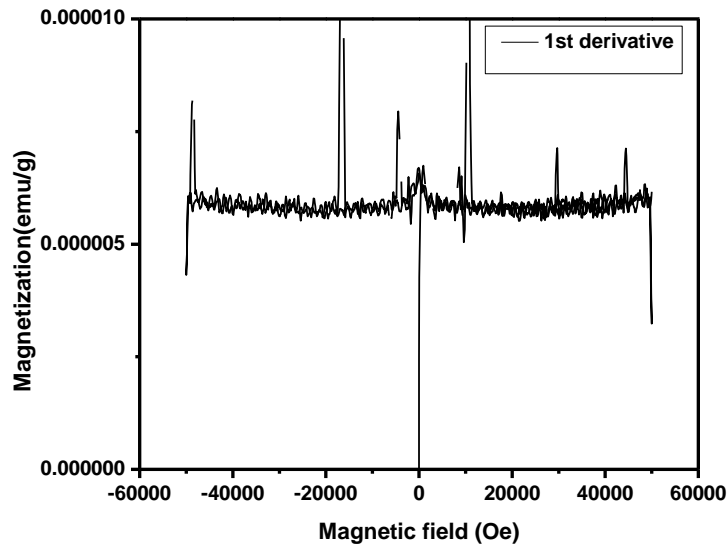


Fig: 4.6 Differential curve of BFO at 5K synthesized by using NH_4OH .

Table 4.2 (b) also shows linear M-H curve at both 5K and 3K and with a slope change in the curve (slope change is larger when compared to the slope change of NH_4OH) which is shown in the figure 4.7.Hence it is anti-ferromagnetic in nature i.e. BFO nanoparticles synthesized using TMAOH exhibits anti-ferromagnetic nature. The loop opening in the curve is may be due to surface defects.

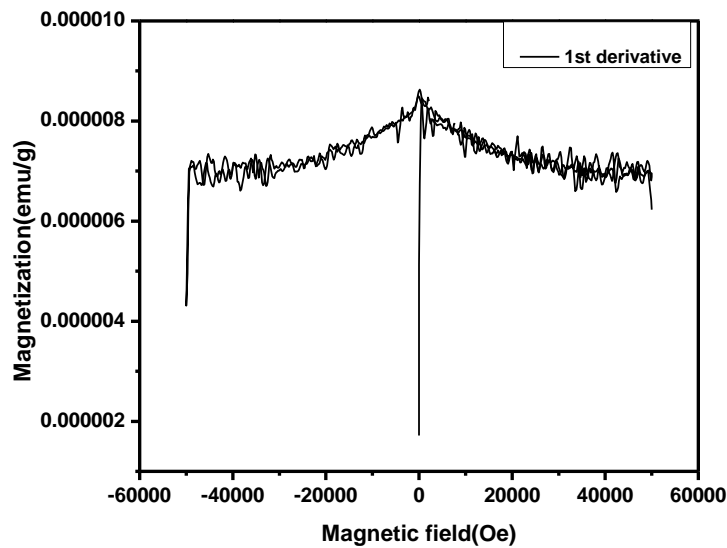


Fig. 4.7: Differential curve of BFO at 5K synthesized by using TMAOH

M-T measurement of BFO nanoparticles synthesized by co-precipitation method using NH_4OH and TMAOH:

Magnetization is measured in the temperature range of 5-300K with an external magnetic field of 1000Oe. In fig 4.8, both FC and ZFC magnetization values decrease with the decrease in temperature which is an indication of anti-ferromagnetic nature [32] similar to bulk behaviour. Because of homogeneity of the particles in the bulk, the blocking effect is not predominant. As a result both FC and ZFC curves coincide.

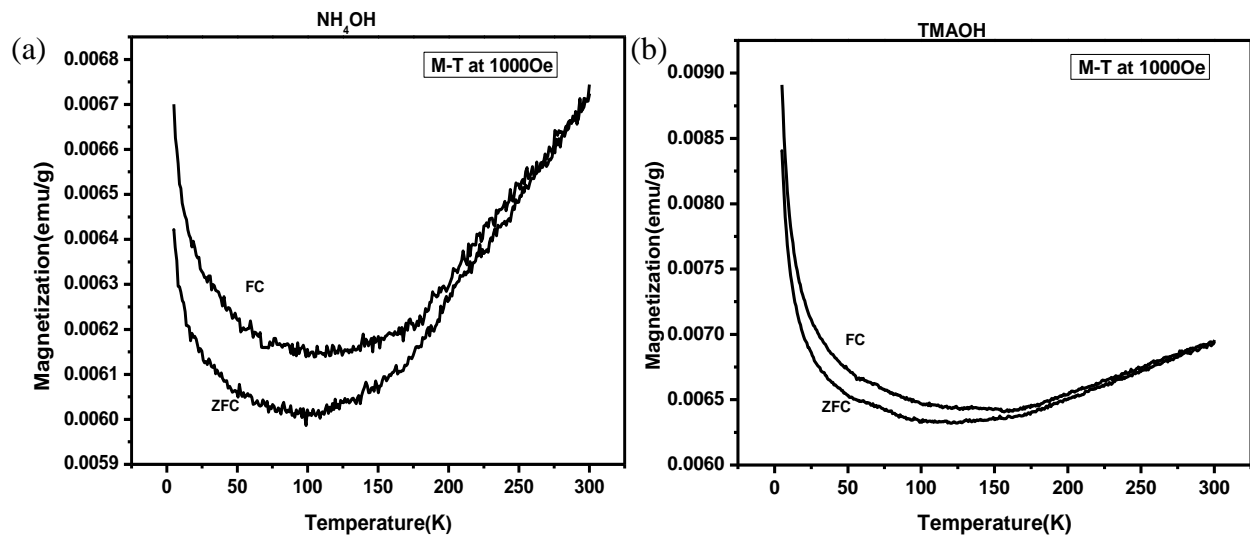


Fig: 4.8: M-T curve of BFO synthesized using (a) NH_4OH and (b) TMAOH at 1000Oe

4.1.4. Raman spectroscopy:

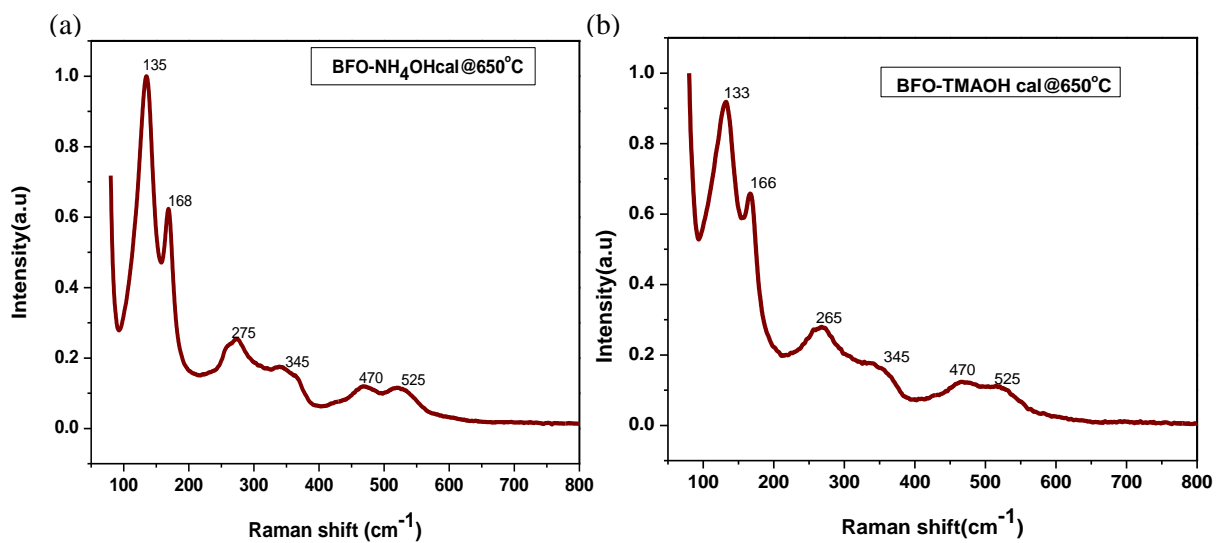


Fig: 4.9 Raman spectra of bismuth ferrite nanoparticles synthesized using (a) NH_4OH and (b) TMAOH.

Single phase BFO nanoparticles are obtained at 650°C in case of both the precipitating agents. The raman spectra are shown in the figure 4.6(a) and (b).

Both the spectra show the 135,133,166,168 265,275,345,470 and 525 modes .According to Aguiar et al. [33]

- ❖ Modes such as 265,275,345,470 and 525 are related to the distortions and vibrations of FeO₆ octahedra.
- ❖ Modes such as 135,133,166,168 are related to bismuth occupied within perovskite units.

Hence raman spectroscopy gives the information regarding the structure. The structure of BFO which is analysed using XRD is further confirmed by raman spectroscopy.

4.2. Synthesis of BFO nanoparticles at constant pH and constant concentration.

4.2.1: Structural analysis by X-Ray diffraction:

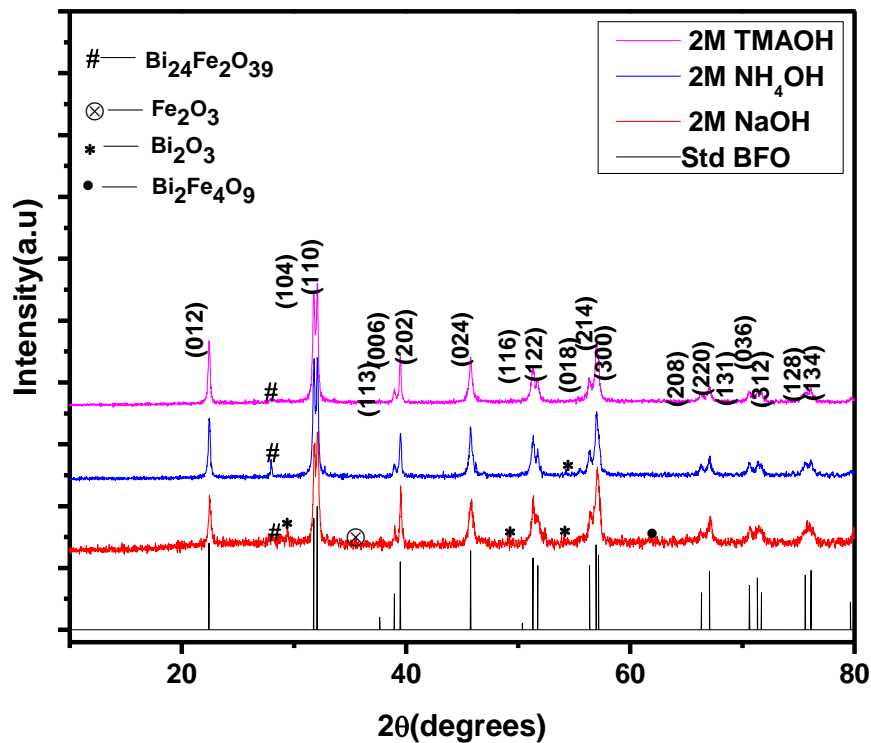


Fig.4.10: XRD patterns of BFO nanoparticles calcined at 550 °C by using (a) 2M-NaOH (b) 2M-NH₄OH and (c) 2M-TMAOH

Figure: 4.10 shows the XRD patterns of BFO nanoparticles synthesized and calcined at 550 °C by co-precipitation method. In this method both the pH and concentration are kept constant in order to determine the role of precipitating agent. The pH-12 and 2M concentration is maintained. The crystallite size is calculated from XRD using Debye-Scherrer formula.

Table-4.3: BFO nanoparticles at constant pH and concentration

Precipitating agent	pH	Concentration	Crystallite size (nm)
NaOH	12	2M	37
NH ₄ OH	12	2M	48
TMAOH	12	2M	48

Table-4.3 shows that the crystallite size of BFO nanoparticles synthesized using 2M NaOH is less compared to BFO nanoparticles synthesized using 2M NH₄OH and 2M TMAOH. This is because NaOH is stronger base when compared to TMAOH. NaOH dissociates faster than TMAOH and NH₄OH and releases hydroxyl ions faster. As a result, large number of particles are formed during nucleation and growth occurs slower. The impurity phases Bi₂₄Fe₂O₃₉, Bi₂O₃, Fe₂O₃ and Bi₂Fe₄O₉ are present in case of NaOH precipitating agent. This is because of uncontrolled precipitation due to faster nucleation. This uncontrolled precipitation makes it inhomogeneous which leads to large amount of impurities.

Chapter-5

Results and discussion of surfactant assisted synthesis of BFO nanoparticles.

5.1 Surfactant:

In this synthesis cetyltrimethylammoniumbromide (CTAB) is used as a surfactant. CTAB is a cationic surfactant and its molecular formula is $C_{19}H_{42}BrN$. It is a molecule with tri methyl ammonium, as a head group and long chain of alkyl group as a tail portion as shown in Figure 5.1

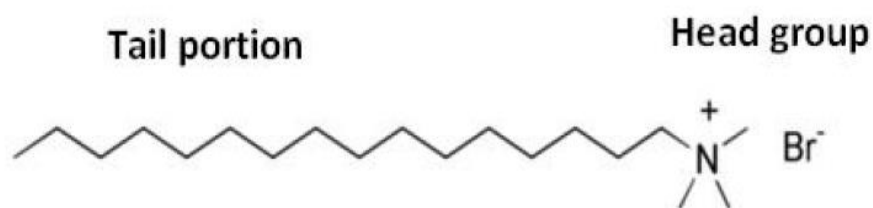


Fig.5.1 Molecular Structure of CTAB [34]

The critical micelle concentration of CTAB is 0.9-1.0mM. Above this concentration CTAB forms micelles which is shown in fig.5.2.

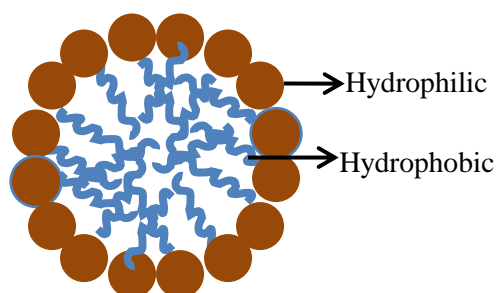


Fig.5.2 Structure of micelle.

Micelle has outer water soluble hydrophilic head and inner water insoluble hydrophobic tail.

5.2. Structural analysis by X-Ray Diffraction:

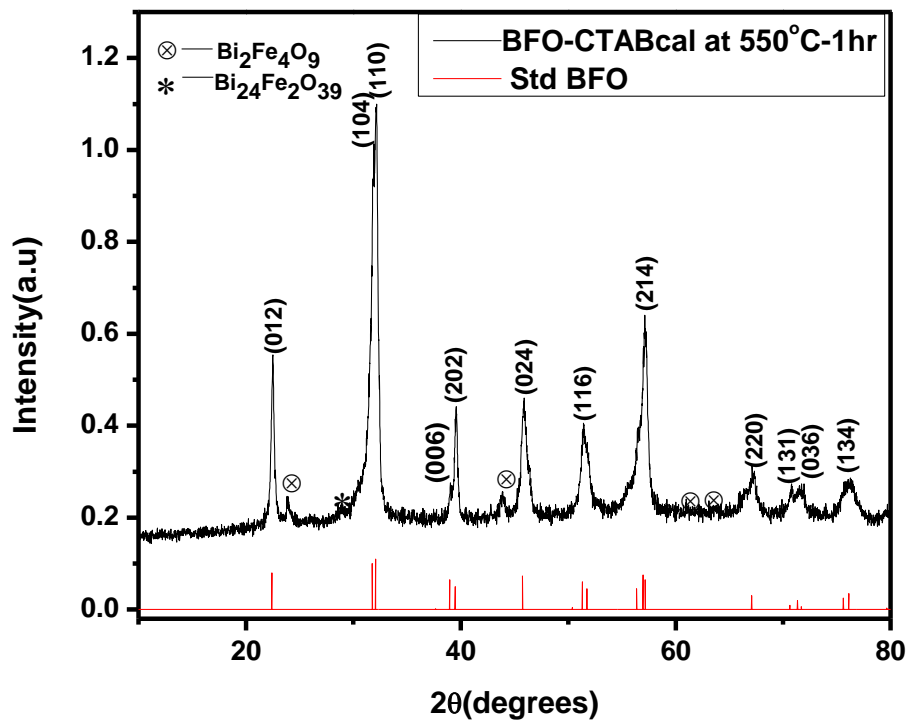


Fig.5.3 XRD pattern of BFO nanoparticles synthesized using CTAB (surfactant) and calcined at 550°C for 1hr

Figure.5.3 shows the xrd pattern of BFO nanoparticles synthesized using CTAB and calcined at 550°C for 1hr. Two impurity phases are seen such as $\text{Bi}_2\text{Fe}_4\text{O}_9$ and $\text{Bi}_{24}\text{Fe}_2\text{O}_{39}$. The crystallite size from Debye-scherrer formula is calculated as 16nm. Compared to crystallite size found in earlier experiments, the crystallite size obtained in this case is much smaller. This can be explained using the below figure.5.4.

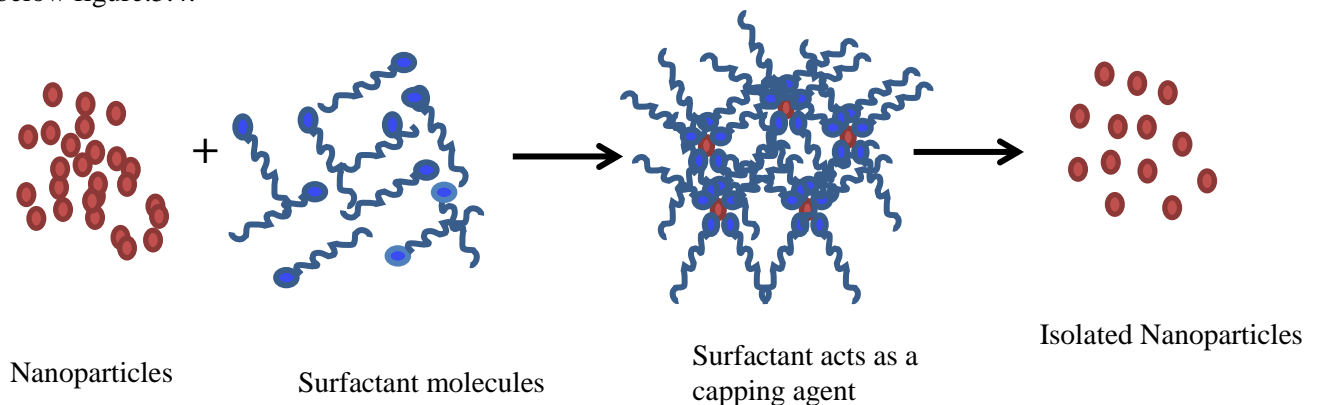


Fig.5.4 Mechanism of CTAB in preventing agglomeration of nanoparticles.

Surfactants are surface-active agents. When surfactant (CTAB) is added to the nanoparticles; it attaches with its head to the nanoparticles and prevents agglomeration among the primary particles by acting as a capping agent. Hence particles without agglomeration are obtained which is shown in fig5.4

In this experiment, smaller crystallite size of BFO was found when CTAB is added. CTAB attaches to BFO nanoparticle with its hydrophilic head which is positively charged and forms an outer shell around BFO nanoparticle. The electrostatic force between positively charged outer shells prevents BFO particles from agglomerating.

5.3. Morphological studies:

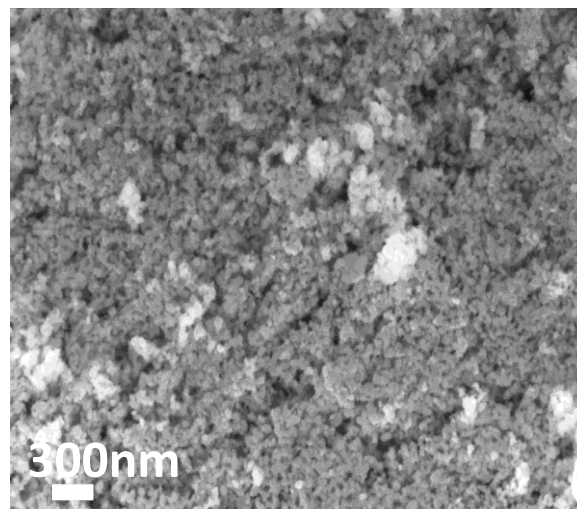


Fig 5.5 FESEM image of BFO nanoparticles synthesized using CTAB surfactant.

Figure: 5.5 shows FESEM image of BFO nanoparticles calcined at 550°C using CTAB Surfactant. It shows smaller particles with average particle size of 59 ± 15 nm calculated using Image J software. This shows that CTAB surfactant plays an important role in preventing the agglomeration of BFO particles by acting as a capping agent

5.4. Magnetic studies:

The magnetic properties of BFO nanoparticles calcined at 550°C using CTAB is performed using PPMS operated in VSM mode. Magnetic measurements were performed at 5K and 300K which is shown in fig 5.6 .M-H curve is hysteresis but not linear indicating weak ferromagnetism. The periodic spiral spin structure which is shown in figure 1.7 is suppressed due to Dzyaloshinskii-Moriya interaction [34] .This suppression results in enhancement of magnetism and therefore M-H curve shows weak ferromagnetic curve. In this case the crystallite size is 16nm, which is less than 64nm; hence it shows weak ferromagnetic nature.

M-H measurements of BFO nanoparticles synthesized by co-precipitation method using CTAB

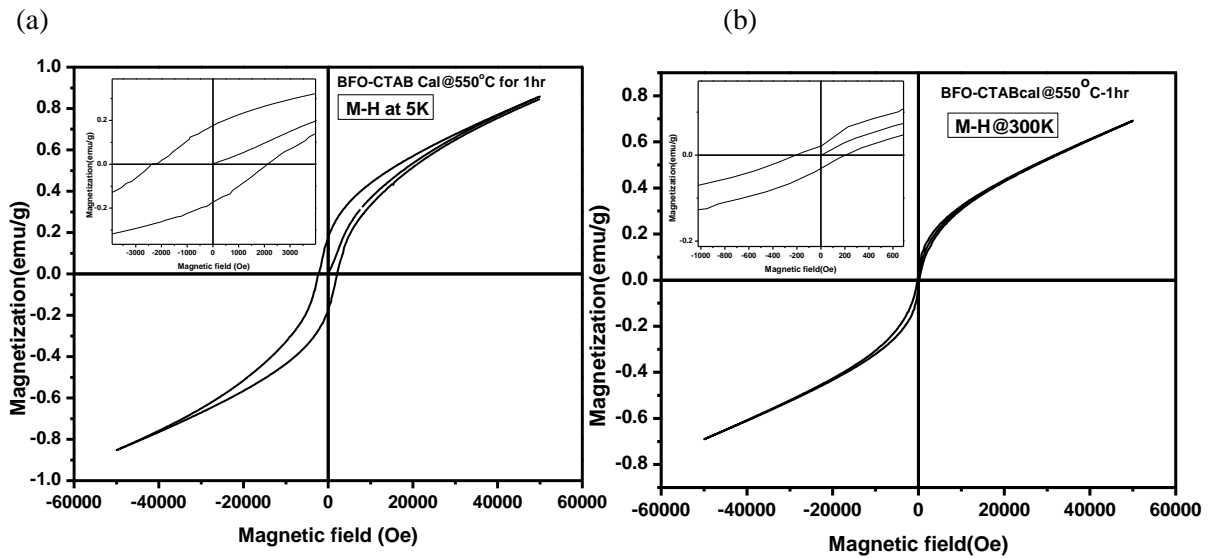


Fig 5.6 M-H curves at (a) 5K and (b) 300K

Table.5.1: Values of magnetization and coercivity.

Precipitating agent+ Surfactant	Average crystallite size(nm)	Remnant magnetization(M_r) (emu/g)		Coercivity (H_c)(Oe)	
		5K	300K	5K	300K
NaOH+ CTAB	16	0.177	0.2635	2255.05	212.3

Table 5.1 shows the values of remnant magnetization and the coercive field at both 5K and 300K. The coercivity value and remnant magnetization value is high at 5K. This is because of the increase in the magnetic ordering at lower temperature and also the presence of impurity phase $\text{Bi}_2\text{Fe}_4\text{O}_9$. The impurity $\text{Bi}_2\text{Fe}_4\text{O}_9$ shows magnetic nature below 273K.

M-T measurement of BFO nanoparticles synthesized by co-precipitation method using CTAB

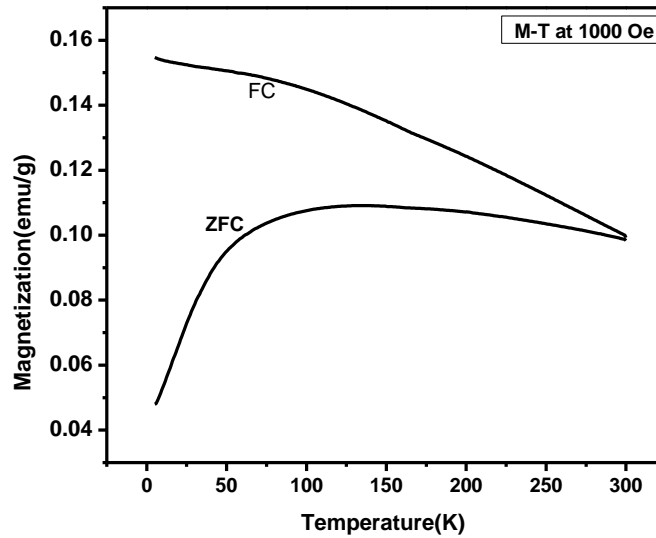


Fig 5.7 M-T curve at 1000Oe

Magnetization is measured in the temperature range of 5-300K with an external magnetic field of 1000Oe. The effect of divergence between ZFC and FC is associated with the blocking effects. T_S (i.e. the temperature where the ZFC and FC starts to bifurcate) is higher for smaller particle than the larger particle [35]. In nanoparticles at temperature $T < T_B$ (the temperature where the magnetization drops is known as blocking temperature) the magnetic moment is blocked due to the higher interactions of nanoparticle clusters because of increase in surface-volume ratio. This causes the difference in FC and ZFC magnetization. The crystallite size in this case is 16nm therefore it shows large bifurcation. ZFC shows sudden drop in magnetization below 100K, indicating blocking effects, however spin-glass type of a transition is expected to appear around 10K for bulk BFO samples, which is not observed prominently in the case of nanoparticles, probably due to the cluster formation of particles [36].

Chapter-6

Results and discussion of BFO Nanofoams synthesized by sol-gel Template method.

6.1 Structural analysis by X-Ray Diffraction:

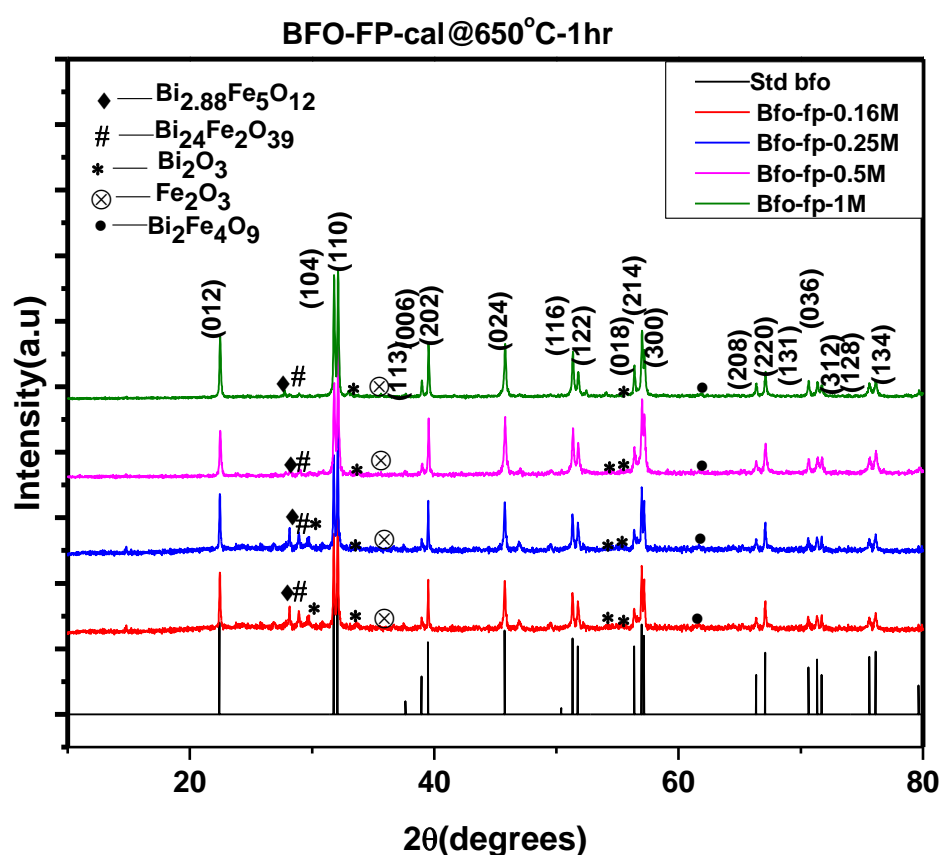


Fig.6.1XRD patterns of BFO Nanofoams synthesized by using different concentrations such as 0.16M, 0.25M, 0.5M and 1M.

Figure: 6.1 shows XRD patterns of BFO Nanofoams synthesized at different metal ion concentrations such as 0.16M, 0.25M, 0.5M and 1M. The impurities such as $\text{Bi}_{2.88}\text{Fe}_5\text{O}_{12}$, $\text{Bi}_{24}\text{Fe}_2\text{O}_{39}$, Bi_2O_3 , Fe_2O_3 and $\text{Bi}_2\text{Fe}_4\text{O}_9$ are present. These impurities are found to decrease from dilute solution to concentrated solution i.e. from 0.16M to 1M. In dilute solution (0.16M) when the solvent is removed

by drying the filter paper in hot air oven; the sol converts to gel i.e. gelation process takes place during drying and which result in inhomogeneity. This inhomogeneity may lead to more impurities. Whereas in concentrated solution (1M) gelation process takes place before drying the filter paper and which makes it homogenous. This homogeneity may lead to decrease in the percentage of impurities. The crystallite size of all the above samples is shown in table 6.1. It shows almost the same crystallite size even there is difference in the concentrations.

Table 6.1: Crystallite size of BFO-FP calcined at 650 °C

BFO calcined at 650 °C	Average crystallite size (nm)
0.16M	103
0.25M	102
0.5M	96
1M	109

XRD of BFO Nanofoam of concentration 0.16M:

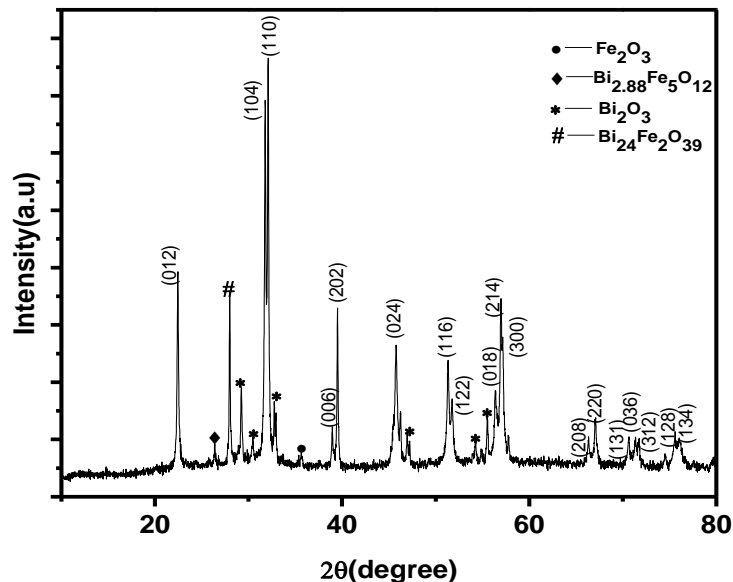


Fig.6.2 XRD pattern of BFO Nanofoam of concentration 0.16M and calcined at 600 °C.

Fig.6.2 shows XRD pattern of BFO Nanofoams synthesized at 0.16M metal ion concentrations, calcined at 600°C. The impurities such as $\text{Bi}_{2.88}\text{Fe}_6\text{O}_{12}$, $\text{Bi}_{24}\text{Fe}_2\text{O}_{39}$, Bi_2O_3 and Fe_2O_3 are present.

6.2: Magnetic studies:

M-H measurements of BFO Nanofoams of 0.16M metal ion concentration synthesized by using sol-gel template method:

Table -6.1 shows values of remnant magnetization (which is expressed in emu/g) and coercivity (in Oe) at both 5K and 300K.

Table: 6.1: Values of magnetization and coercivity at 5K and 300K

Concentration of metal ion	Crystallite size(nm) at 600°C	Remnant magnetization(M_r) (emu/g)		Coercivity (H_c)(Oe)	
		5K	300K	5K	300K
0.16M	55	2.142	0.781	668.04	192.01

Magnetic measurements were performed for BFO Nanofoams of 0.16M, calcined at 600°C. Magnetic measurements were done at both 5K and 300K. It shows hysteresis curve but not linear at both 5K and 300K, which is shown in figure 6.4. It shows larger slope change which is shown in figure 6.4, indicating weak ferromagnetism. This enhanced magnetization is could be due to the presence of Fe_2O_3 impurity phase [37]

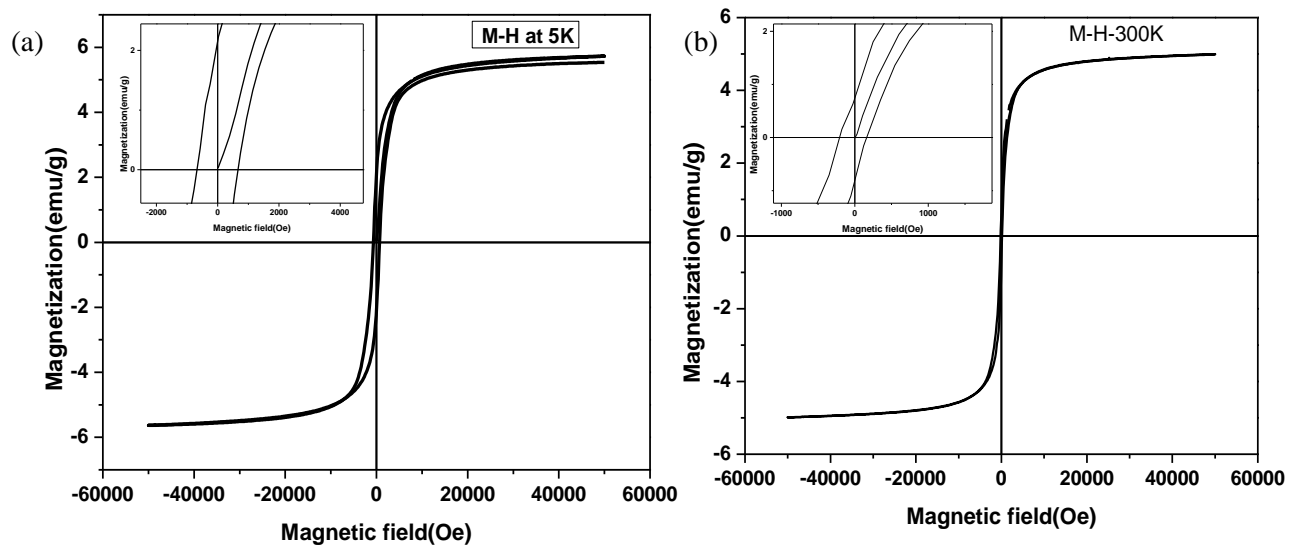


Fig 6.3 M-H curves of 0.16M concentration of (a) 5K and (b) 300K, calcined at 600°C.

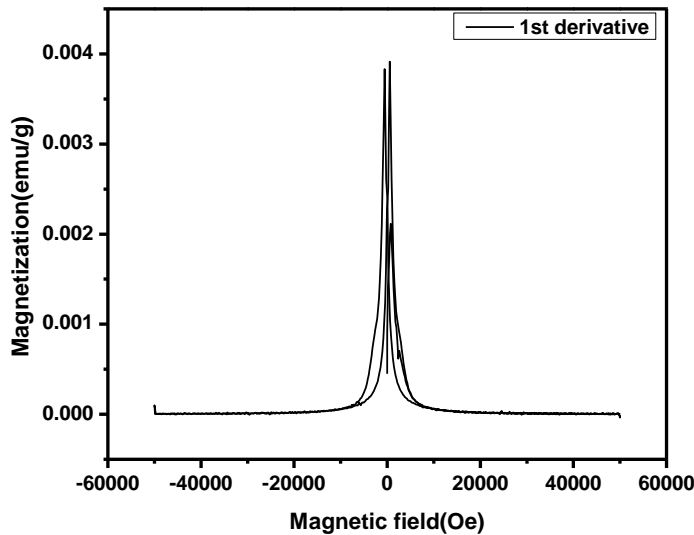


Fig 6.4: Differential curve of BFO Nanofoam of 0.16M which is calcined at 600 °C

M-T measurement of BFO Nanofoams of 0.16M concentration of metal ion synthesized by using sol-gel template method:

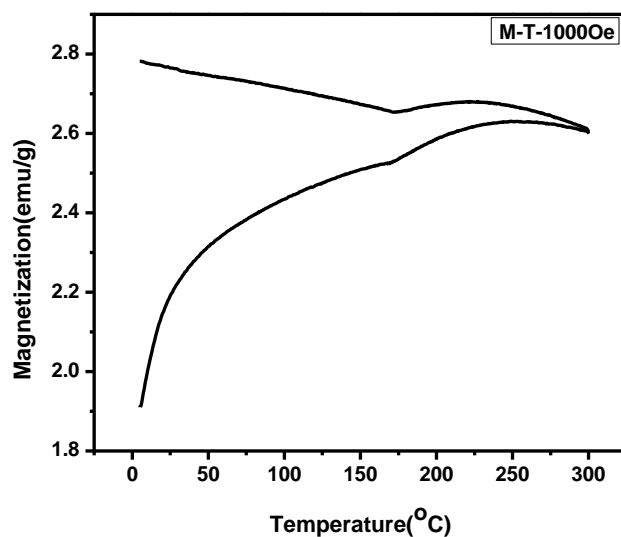


Fig 6.5: M-T curve of BFO Nanofoam of 0.16M which is calcined at 600 °C

Magnetization is measured in the temperature range of 5-300K with an external magnetic field of 1000Oe. The effect of divergence between ZFC and FC is associated with the blocking effects. T_S (i.e. the temperature where the ZFC and FC starts to bifurcate) is higher for smaller particle than the larger particle. ZFC shows sudden drop in magnetization below 100K, indicating blocking effects.

6.3 Morphological studies:

Figure: 6.5 shows FESEM images of BFO Nanofoams synthesized by using different concentrations of metal ions such as (a) whatman filter paper (b) 0.16M (c) 0.25M and (d) 0.5M. We found that there is no change in the crystallite size from 0.16M to 0.5M, but there is a change in porosity which is shown in fig 6.6. Porosity decreases from dilute solution (0.16M) to concentration solution (0.5M). In the case of dilute solution, the volume is high and the coating of the material on the filter paper is thin. So when the material is converting from the amorphous to the crystalline only in the parts where the material is present converts to crystallite and other parts are empty with only the filter paper. During calcination the filter paper decomposes which leads to the formation of pores. Hence the particle shape is not spherical but plate like structure.

In the case of concentrated solution (0.5M), the volume is less and hence coating is thick. This makes the material homogenously distribute on the filter paper. When the material is converting from the amorphous to the crystalline, most of the material converts to crystalline which makes it less porous. In this case the template is playing a role in crystallization process of the material.

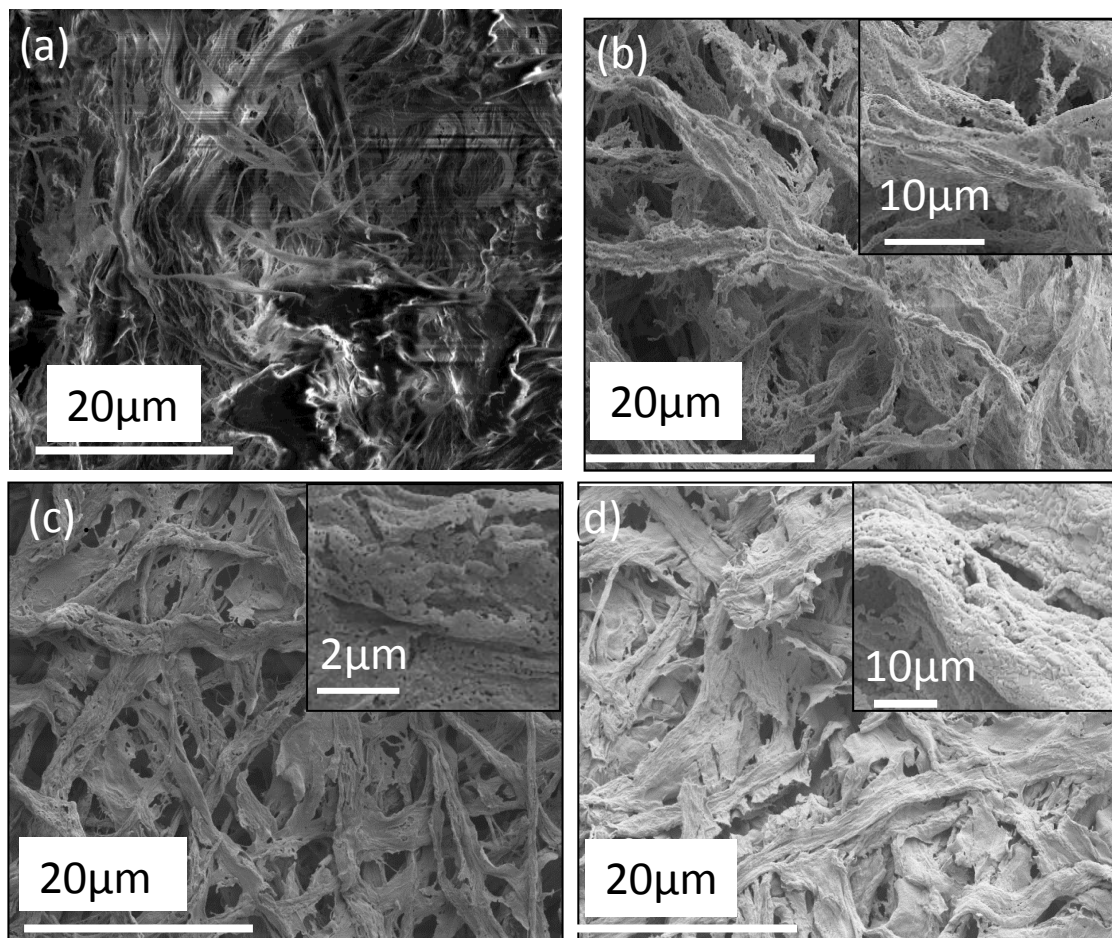


Fig 6.6: FESEM images of BFO Nanofoams (a) whatman filter paper (b) 0.16M (c) 0.25M and (d) 0.5M.

Chapter-7

Summary and Conclusions

In this project work an attempt has been made to understand the kinetics of phase formation of BFO via wet chemical route. We studied the effect of synthesis parameters such as pH, concentration, precipitating agents, surfactant etc., in determining the single phase formation of BFO and analyzed the structural, morphological and physical properties with XRD, Raman spectroscopy, SEM and PPMS(operated in VSM mode).By tuning the above conditions, different particle sizes and shape (morphology) was synthesized

- ✓ Difference in basicity and concentration of precipitating agents affects crystallite size, impurity content and phase evolution of single phase BFO.
 - Stronger base showed smaller crystallite size and large amount of impurities at lower calcination temperatures.
 - High concentration of a weak base showed larger crystallite size.
- ✓ Using CTAB as a surfactant lead to significant reduction in crystallite size which suppressed the spiral spin structure present in bismuth ferrite. Hence resultant BFO particles showed weak ferromagnetic nature.
- ✓ Synthesized BFO Nanofoams using whatman filter paper as a template by sol-gel method. Results in no change in the crystallite size from 0.16M to 1M concentrations of metal ion but there is a change in porosity.Porosity decreases from dilute solution (0.16M) to concentration solution (0.5M).In the case of concentrated solution, the template plays an important role in crystallization process of the material. As a result the particles shapes are not spherical but are plate like structure.

Future work:

1. Synthesis of pure phase BFO Nanofoam and study its magnetic properties.
2. To study the ferroelectric properties of BFO synthesized by the above methods, since BFO is a multiferroic material (ferroelectric- antiferromagnetic)

References:

- [1] L.W.Martin, S.P.Crane, Y.H.Chu, M B Holcomb, M Gajek, M.Huijben, C.H.Yang, N.Balke and R.Ramesh. Multiferroics and magnetoelectrics: thin films and nanostructures. *Journal of Physics: Condensed Matter* 20, (2008) 434220.
- [2] K.F.Wang, J.M.Liu and Z.F.Ren. Multiferroicity: the coupling between magnetic and polarization orders. *Advances in Physics* 58, (2009) 321–448.
- [3] L.W.Martin. D.G.Schlom. Advanced synthesis techniques and routes to new single-phase Multiferroics. *Current Opinion in Solid State and Materials Science* 16, (2012) 199–215.
- [4] D.I.Khomskii .Classifying multiferroics, *physics* 2, (2009) 20.
- [5] J.V.Brink and D.I.Khomskii .Multiferroicity due to charge ordering. *Journal of Physics: Condensed Matter* 20, (2008) 434217.
- [6] M.Staruch, D.Violette and M. Jain. Structural and magnetic properties of multiferroic bulk TbMnO_3 . *Materials Chemistry and Physics* 139, (2013) 897-900.
- [7] S.K.Srivastav and N S.Gajdhiye. Low temperature synthesis, structural, optical and magnetic properties of bismuth ferrite nanoparticles. *Journal of American and Ceramic Society* 95, (2012) 3678-3682.
- [8] H.Shokrollahi. Magnetic, electrical and structural characterization of BiFeO_3 nanoparticles synthesized by co-precipitation. *Powder Technology* 235, (2013) 953–958.
- [9] H.Naganuma. *Ferroelectrics-Physical effects*. Mickael Lallart, 2011.
- [10] R.Safi and H.Shokrollahi. Physics, chemistry and synthesis methods of nanostructured bismuth ferrite (BiFeO_3) as a ferroelectro-magnetic material. *Progress in Solid State Chemistry* 40, (2012) 6-15.
- [11] M.YShami, M.S.Awan and M.Anis-ur-Rehman. Phase pure synthesis of BiFeO_3 nanopowders using diverse precursor via co-precipitation method. *Journal of Alloys and Compounds* 509, (2011) 10139-10144.
- [12] A.R.West.*Solid state chemistry*. John wiley & sons, 1985.
- [13] J.Wei, D.Xue. Low-temperature synthesis of BiFeO_3 nanoparticles by ethylenediaminetetraacetic acid complexing sol–gel process. *Materials Research Bulletin* 43 (2008) 3368–3373.

- [14] C.Chen, J.Cheng, S.Yu, L.Che, and Z.Meng. Hydrothermal synthesis of perovskite bismuth ferrite crystallites. *Journal of Crystal Growth* 291 (2006) 135–139
- [15] S.N.Tripathy, B.G.Mishra, M M.Shirolkar, S.Sen, S.R.Das, D B.Janes, D.K.Pradhan. Structural, microstructural and magneto-electric properties of single-phase BiFeO₃ nanoceramics prepared by auto-combustion method. *Materials Chemistry and Physics* 141 (2013) 423-431.
- [16] Z.Liu, Y.Qi and C.Lu. High efficient ultraviolet photocatalytic activity of BiFeO₃ nanoparticles synthesized by a chemical coprecipitation process. *Journal of Materials Science:Materials in Electronics*, 21 (2010) 380–384.
- [17] M.Vijayakumar. Development of rare earth based lithium silicates and nanocomposite polymer solid electrolytes for lithium battery applications. Ph.D thesis. Pondicherry University, 2010
- [18] H.Ke, W.Wang, Y.Wang, J.Xu, D.Jia, Z.Lu, and Y.Zhou. Factors controlling pure-phase multiferroic BiFeO₃ powders synthesized by chemical co-precipitation. *Journal of Alloys and Compounds*, 509 (2011) 2192–2197.
- [19] G. Catalan and J. F. Scott. Physics and applications of Bismuth Ferrite. *Advanced Materials*, 21 (2009), 2463–2485.
- [20] H.Mirabbos, X.Yunhua, W.Fazhan, J Wang, L.Wengang and W.Mingiong. Morphology-controlled hydrothermal synthesis of Bismuth ferrite using various alkaline mineralizers. *Ceramics – Silikaty*, 53 (2009) 113-117.
- [21] A.Y.Kim, S.H.Han, H-W.Kang, H-G.Lee, J.S. Kim, and C.I.Cheon. Dielectric and magnetic properties of BiFeO₃ ceramics prepared by hydrothermal synthesis. *Ceramics International*, 38S (2012) S397–S401
- [22] M.kisku. Surfactant assisted autocombustion synthesis of Bismuth Ferrite. B.Tech thesis, National institute of technology Rourkela, 2009
- [23] Y.Fenfang. Template-assisted synthesis and assembly of nanoparticles. Ph.D thesis, National University of Singapore (NUS), 2008.
- [24] J.Wei, D.Xue and Y.Xu. Photoabsorption characterization and magnetic property of multiferroic BiFeO₃ nanotubes synthesized by a facile sol–gel template process. *Scripta Materialia* 58 (2008) 45–48.
- [25] X.Y.Zhang, C.W.Lai, X.Zhao, D.Y.Wang, and J.Y.Dai. Synthesis and ferroelectric properties of multiferroics BiFeO₃ nanotube arrays. *Applied Physics Letters*, 87 (2005) 143102.
- [26] L.A.S.de Oliveira, K.R.Pirota. Synthesis, structural and magnetic characterization of highly ordered single crystalline BiFeO₃ nanotubes. *Materials Research Bulletin* 48 (2013) 1593–1597.
- [27] Y.Huo, Y.Jin, Y.Zhang. Citric acid assisted solvothermal synthesis of BiFeO₃ microspheres with high visible-light photocatalytic activity. *Journal of Molecular Catalysis A: Chemical*, 331 (2010) 15–20

- [28] B.D.Cullity. Elements of X-Ray Diffraction. Addition Wesley, 1956.
- [29] R.Egerton. Physical Principles of Electron Microscopy. 1st edition, springer, 2005.
- [30] S.Mahalaxmi. Structure, electrical and magnetic properties of rare earth doped nanophase ferrites. Ph.D thesis, Pondicherry University, 2010.
- [31] A.Gajovic, S.Sturm, B.JanWar, A.Santic, J.k.Zagar, and M.Ceh. The Synthesis of pure-phase Bismuth Ferrite in the Bi–Fe–O system under hydrothermal conditions without a mineralizer. Journal of the American Ceramic Society, 93 (2010) 3173–3179.
- [32] D.P.Dutta, B.P.Mandal, R.Naik, G.Lawes, and A.K.Tyagi. Magnetic, ferroelectric, and magnetocapacitive properties of sonochemically synthesized Sc-doped BiFeO₃ Nanoparticles. Journal of Physical. Chemistry. C, 117(2013), 2382–2389.
- [33] E.C.Aguiar, M.A.Ramirez, F.Moura, J.A.Varela, E.Longo and A.Z.Simoes .Low-temperature synthesis of nanosized bismuth ferrite by the soft chemical method. Ceramics International 39 (2013) 13-20
- [34] T.J.park, G.C.Papaefthymiou, A.J.Viescas, A.R.Moodenbaugh, and S.S.Wong. Size-dependent magnetic properties of single crystalline Multiferroic BiFeO₃ Nanoparticles, Nanoletters, 7 (2007).766-722.
- [35] K.D.Nisha. Synthesis and characterization of organic molecules passivated cadmium sulphide nanostructures for biological applications. Ph.D thesis, SRM University, 2003.
- [36] V.A.Reddy, N.P.Pathak and R.Nath. Particle size dependent magnetic properties and phase transitions in multiferroics BiFeO₃ nano-particles. Journal of Alloys and Compounds 543 (2012) 206–212.
- [37] B.Ramachandran and M.S.Ramachandra Rao. Low temperature magnetocaloric effect in polycrystalline BiFeO₃ ceramics. Applied Physics Letters. 95,(2009), 142505.
- [38] M.Sakar, S.Balakumar, P.Saravanan and S.N.Jaisankar. Manifestation of weak ferromagnetism and photocatalytic activity in Bismuth Ferrite nanoparticles. American institute of physics, 1512 (2013), 228-229.